

One Extension to Explain Them All, One Parameter to Minimize χ^2 , One Framework to Bring Them All, and in One Model Bind Them

Matteo Forconi^{1, 2,*} and Eleonora Di Valentino^{2, †}

¹*Physics Department and INFN sezione di Ferrara,
Università degli Studi di Ferrara, via Saragat 1, I-44122 Ferrara, Italy*

²*School of Mathematical and Physical Sciences, University of Sheffield,
Hounsfield Road, Sheffield S3 7RH, United Kingdom*

(Dated: March 7, 2025)

The increasing precision of Cosmic Microwave Background (CMB) observations has unveiled significant tensions between different datasets, notably between Planck and the Atacama Cosmology Telescope (ACT), as well as with late-Universe measurements of the Hubble constant. In this work, we systematically explore a variety of beyond- Λ CDM extensions to assess their ability to reconcile these discrepancies. Specifically, we consider modifications to the primordial power spectrum ($n_s = 1$, $\alpha_s \neq 0$), geometry ($\Omega_k \neq 0$), dark energy ($w \neq -1$), the effective number of relativistic species ($N_{\text{eff}} \neq 3.044$), and the primordial helium fraction (Y_p), as well as an Early Dark Energy (EDE) component. We evaluate each model using multiple statistical tools, including the Akaike Information Criterion (AIC), Bayesian model comparison, suspiciousness, and the goodness-of-fit estimator Q_{DMAP} . Our results confirm that no single extension fully resolves all existing tensions. While a nonzero curvature is favored by Planck-only data, it does not alleviate the Planck-ACT discrepancy. The EDE scenario, particularly with a fixed Harrison-Zel'dovich spectrum ($n_s = 1$), provides the best resolution to the Planck-ACT inconsistency, while w CDM is more effective at reducing the Hubble tension when SH0ES data are included. However, the statistical preference for these extensions remains moderate, and imposing $n_s = 1$ often worsens model performance. Our findings highlight the limitations of incremental modifications to Λ CDM and suggest that either more complex new physics or, more likely, improved systematic understanding in the CMB sector may be required to fully address the observed tensions. While CMB experiments are often considered the gold standard of precision cosmology, our results reinforce that these measurements are not immune to systematic uncertainties, which may be underestimated in current analyses.

I. INTRODUCTION

The Cosmic Microwave Background (CMB) provides one of the strongest observational pillars of modern cosmology. Ever since the COBE satellite's first measurements of the CMB's nearly perfect black-body spectrum and tiny temperature fluctuations [1, 2], researchers have steadily refined these observations through missions such as WMAP [3, 4] and, more recently, Planck [5], the Atacama Cosmology Telescope (ACT) [6, 7], and the South Pole Telescope (SPT) [8–10]. These data sets allow the construction of a standard model of cosmology: Λ CDM, in which a spatially flat Universe is dominated at late times by a cosmological constant, Λ , and cold dark matter (CDM). Furthermore, in the early epochs, the Universe experienced a phase of exponential acceleration, the so-called inflationary epoch [11], which is responsible for large-scale homogeneity and the generation of primordial density fluctuations. However, it is important to underline that Λ CDM remains a phenomenological framework containing three major unknown ingredients— inflation, dark matter, and dark energy—whose theoretical motivations still lack direct experimental confirmation.

Over the last decade, as the precision of cosmological

measurements has improved, several intriguing discrepancies have emerged [12–14]. The most significant is the so-called Hubble tension [15–28], a $> 5\sigma$ mismatch between the Hubble constant measured via late-Universe probes [29–53] and the smaller H_0 value inferred from early-Universe observations [5, 7], under the assumption of Λ CDM. Moreover, Planck data itself exhibit other anomalies, including an enhanced CMB lensing amplitude at about 2.8σ [5, 54–64] and a preference for a closed geometry at roughly 3.4σ [5], introducing an inconsistency with Baryon Acoustic Oscillation (BAO) data [65–72]. Collectively, such anomalies raise the question of whether new physics beyond Λ CDM is needed or whether there are some unrecognized systematic errors in one or more datasets.

An additional layer of tensions arises from comparing multiple independent CMB data sets. While the Planck satellite has provided the tightest constraints to date, ACT can offer valuable confirmation of Planck cosmology. Intriguingly, although ACT generally agrees with Planck, small discrepancies appear. For instance, analyses have found a mild-to-moderate tension at the $\sim 2.5\sigma$ level between Planck and ACT [73–77], particularly in the inferred values of the spectral tilt n_s [78–82], but also in the effective number of relativistic degrees of freedom [83], the running and the running of the running of the spectral index [7, 84], the neutrino mass [85], the evidence for Early Dark Energy [86, 87], and for Dynamical

* matteo.forconi@fe.infn.it

† e.divalentino@sheffield.ac.uk

Dark Energy [88].

These developments underline the importance of assessing the consistency of independent CMB measurements [73, 89–91] and their compatibility with external late-Universe observations such as SH0ES. In this work, we analyze different extensions to the standard cosmological scenarios using multiple statistical metrics. We investigate how these models perform in light of the Hubble tension and the Planck vs. ACT discrepancy, aiming to find a unique solution.

This paper is organized as follows. Sec. II is dedicated to presenting the alternative cosmological models. Sec. III describes the statistical metrics used in the analyses. Sec. IV presents the methodology and the dataset, whereas in Sec. V, we present our results. We conclude in Sec. VI.

II. BATTLE GROUNDS

In this paper, we aim to study the consistency between Planck and ACT observations within different scenarios. Before proceeding to analyze the different extra parameters we choose to employ, it is important to stress that there are mainly two indicators of the discrepancy between these two CMB experiments: the spectral index, $n_s^{\text{Planck}} = 0.9649 \pm 0.0044$ [5] vs. $n_s^{\text{ACT}} = 1.008 \pm 0.015$ [7], and the baryon energy density, $\Omega_b^{\text{Planck}} h^2 = 0.02236 \pm 0.00015$ [5] vs. $\Omega_b^{\text{ACT}} h^2 = 0.02153 \pm 0.00030$ [7]. These differences persist even when accounting for the lack of small-multipole (\sim first two acoustic peaks) observations from ACT [7, 92] or its limited amount of polarization data (only for n_s) [92], as well as when including non-CMB data [7, 92]. Although observational systematic errors and statistical fluctuations may provide an explanation, we aim to explore the possibility that a limitation of the standard cosmological model is the root of this tension.

The idea behind choosing the alternative models is that they should impact either n_s or $\Omega_b h^2$, such that a natural shift occurs that might ease the tension. Furthermore, to better study the behavior of the consistency between Planck and ACT, quantified by the statistical tools described in Sec. III, we also force $n_s = 1$ for each case, as explained below. By reducing the number of parameters in the model, we accommodate ACT predictions for the spectral index and test the ability of Planck observations to compensate. On the other hand, we also move in the opposite direction (towards Planck predictions) by imposing a tight bound on the helium fraction, forcing higher values of $\Omega_b h^2$ with respect to ACT observations in one realization.

The proposed *battle grounds* to study this inconsistency range from early- to late-Universe solutions. This is because Planck shows a moderate deviation from ΛCDM when extending the latter, while in contrast, ACT shows anomalies in the former [24]. Although the large experimental uncertainties in the late-time sector suggest that

the discrepancy between the two probes could stem from an inconsistency in the early Universe, we include late-time solutions for two main reasons: first, to explore the possibility that this anomaly is somehow linked to the Hubble tension and determine whether any of the beyond- ΛCDM phenomenology studied can increase the present-day expansion rate of the Universe while also leading to an agreement between the two CMB probes; and second, because for each model, we also impose $n_s = 1$, thereby introducing a modification at early times.

1. Primordial Power Spectrum

A general prediction of inflationary theory is that the power spectrum of density perturbations can be well described by a power law $\propto k^{n_s}$, where n_s is the scalar spectral index. The value of the spectral index should be nearly (but not exactly) one due to the dynamics of the inflaton field. This contrasts with the phenomenological model of the early Universe that fixes the scalar spectral index to $n_s = 1$, the so-called Harrison-Zeldovich (HZ) spectrum [93–95]. Although it is possible to recover the HZ spectrum in specific inflationary models (e.g., [96–99]), generally, a value of $n_s \neq 1$ is considered strong evidence in favor of inflationary theory. For example, tensor modes in the CMB are a unique prediction of inflationary theory, and their amplitude is expected to be proportional to the square of the deviation from scale invariance, $|n_s - 1|^2$. Furthermore, as shown in [78, 80, 100, 101], a shift in n_s is related to a shift in H_0 as $\delta n_s \simeq 0.4 \delta H_0 / H_0$, assuming a non-modified recombination process and a late-time ΛCDM framework. From this perspective, we can argue that an HZ spectrum could provide a solution to the Hubble tension.

The latest CMB observations provided by *Planck* exclude an HZ spectrum at more than 8σ [5, 102, 103], corroborating inflationary theory. On the other hand, the ACT collaboration shows deviations from the ΛCDM scenario [75, 77, 83], including a discrepancy in the scalar spectral index, which is consistent with 1 within one σ ($n_s = 1.008 \pm 0.015$ [7]). This represents a new potential challenge for inflationary cosmology: is canonical inflation the dominant mechanism for producing the perturbations in the early Universe? The role of this new tension in the spectral index could be related to systematic effects or could play a prominent role in our understanding of the Universe [78–81, 92, 104–107].

In the standard ΛCDM model, the spectral index is assumed to be scale-independent. This means neglecting the next-order correction terms from the Taylor expansion around the pivot scale k_* and considering the spectrum of primordial perturbations as the power law:

$$\Delta^2(k) = A_s \left(\frac{k}{k_*} \right)^{n_s - 1}. \quad (1)$$

However, inflation does not predict a precise value for the spectral index. This depends on the details of the

inflationary dynamics and the shape of the potential. For this reason, we can expand Eq. (1) to the next order:

$$\Delta(k) = \Delta(k_*) + \frac{d\Delta(k)}{d \log k} \Big|_{k_*} \log\left(\frac{k}{k_*}\right) + \frac{1}{2} \frac{d^2\Delta(k)}{d \log k^2} \Big|_{k_*} \log^2\left(\frac{k}{k_*}\right) + \dots \quad (2)$$

and define the running of the spectral index α_s [108–112]¹ as

$$\alpha_s \equiv \frac{dn_s}{d \ln k} \Big|_{k_*}, \quad (3)$$

which quantifies the rate of change of n_s per Hubble time. Planck observations [5] provide a running compatible with zero, $\alpha_s = -0.006 \pm 0.013$ at 68% CL, which maintain its compatibility when combined with other probes [84, 115–118]. The constraints are slightly relaxed for ACT and SPT-3G [75, 84, 92, 119, 120], but still favor a scale-independent spectral index at 2σ , as also suggested by forecasts of future experiments [121, 122].

2. Late Dark Energy

Since our Universe is accelerating [123–127], the dominant component of our Universe today must be characterized by a negative pressure, so that it can counterbalance the natural decelerated expansion. This component is called Dark Energy ($\sim 70\%$ of the total content), and in the standard model of cosmology, it is parametrized by a positive cosmological constant, Λ . Λ has an equation of state:

$$w = \frac{p}{\rho} = -1 \quad (4)$$

which satisfies the negative-pressure requirement ($w < -1/3$).

An alternative to the cosmological constant Λ is to relax Eq. (4) and assume a generic fluid with a constant equation of state w . By extending ΛCDM to $w\text{CDM}$, that is, introducing w as an extra parameter, it is possible to test the validity of ΛCDM . With w now a free parameter, aside from recovering ΛCDM when $w = -1$, we can explore two different regimes: the *phantom regime* [128–133], characterized by $w < -1$ and a possible violation of the null energy condition (although it is possible for the equation of state to be effectively phantom without violating the null energy condition), and the *quintessence regime* [134–138]. Planck data suggest a DE component in the phantom regime at $\lesssim 2\sigma$, with $w = -1.58^{+0.52}_{-0.41}$ at 95% CL [5], and this preference is maintained when combined with other probes [139–153], while ACT is consistent with $w = -1$ but with large uncertainties ($w = -1.18^{+0.40}_{-0.55}$ at 68% CL) [24, 75].

3. Universe Geometry

Spatial curvature is usually parameterized by the curvature energy density parameter Ω_k , which affects the Hubble expansion rate with a redshift dependence $\propto (1+z)^2$. In modern cosmology, it has become common practice among phenomenologists and observers to consider the curvature parameter as optional, setting $\Omega_k = 0$ and reducing to the standard six-parameter ΛCDM concordance cosmology. This approach is strongly motivated by inflationary theory [11, 154, 155]. An exponential expansion during an inflationary phase drives the Universe towards flatness; in this phase, $\Omega_k = 0$ is a late-time attractor and suppresses any primordial spatial curvature [11]. However, fixing this parameter is akin to assuming a delta-function prior on a phenomenological parameter, which consequently alters the cosmological constraints. For this reason, it is important to have a solid justification for it [72].

Curvature constraints from SPT-3G 2018 alone [10] and ACT+WMAP [7] are fully consistent with a flat Universe. However, Planck data alone suggest a possible detection of a closed Universe (i.e., $\Omega_k < 0$) at over 2σ [5]. To break the geometric degeneracy [156] that CMB experiments face when exploring curvature, temperature and polarization data are combined with late-time measurements such as Baryon Acoustic Oscillations (BAO) [157, 158]. This joint analysis reduces (and often eliminates) the preference for a negative curvature parameter, at the cost of combining experiments that are in tension at more than 3σ (see e.g., [65, 71, 159]). Some argue that the indication of a closed Universe arises from a prior problem in the exploration of parameter space with curvature [160, 161]. Conversely, the assumption of a flat Universe is reinforced when the HillPoP likelihood is used [162].

Curvature can also be assessed through its effects on the late-time Universe alone. When flatness is not assumed in the fiducial model, CMB-independent analyses of low-redshift data do not provide compelling evidence for either a closed or flat Universe [69, 70, 163–165]. However, future analyses employing model-independent approaches may help resolve this conundrum [166].

4. Helium Abundance

As fixing the spectral index exacerbates the tension in the baryon fraction of the Universe, we aim to test the tension between the two datasets by allowing the Helium fraction to vary freely. First, we simply apply a flat prior and refer to this extension as $\Lambda\text{CDM}+Y_p$. Then, we impose a prior on the primordial Helium mass fraction based on $Y_p = 0.2446 \pm 0.0029$ [167], derived from H II region observations, which is similar to another widely used

¹ Similarly, you can define it for the tensor index, see, e.g., [113, 114]

independent measurement, $Y_p = 0.2449 \pm 0.0040$ [168];² we denote this model as Λ CDM+BBN.

Introducing this parameter breaks the BBN relation [169]:

$$\Omega_b h^2 = \frac{1 - 0.007125 Y_p^{\text{BBN}}}{273.279} \left(\frac{T_{\text{CMB}}}{2.7255 K} \right)^3 \eta_{10} \quad (5)$$

where $\eta_{10} \equiv 10^{10} n_b / n_\gamma$ is the photon-baryon ratio today, T_{CMB} is the CMB temperature at the present time, and $Y_p^{\text{BBN}} \equiv 4n_{\text{He}} / n_b$ is the helium *nucleon fraction*. The helium *mass fraction* Y_p , used in our extensions, is recovered via the relation:

$$Y_p = \frac{Y_{He4} m_{He4}}{Y_{He4} m_{He4} + (1 - 4Y_{He4}) m_{H1}} \quad (6)$$

with $Y_{He4} = 1/4Y_p^{\text{BBN}}$, $m_{He4} \simeq 4.0026$, and $m_{H1} \simeq 1.0078$.

5. Effective Number of Relativistic Degrees of Freedom

With the expansion of the Universe, the temperature drops below the electron mass ($T \sim 0.5$ MeV), initiating pair annihilation between electrons and positrons. This results in the production of two photons with a subsequent injection of energy. Such an increase in energy does not affect neutrinos, as they decouple at $T_\nu \sim 1$ MeV [170–172] and therefore no longer share the same temperature, with $T_\nu \neq T_\gamma$. Specifically, they are related via

$$T_\nu = \left(\frac{4}{11} \right)^{\frac{1}{3}} T_\gamma \quad (7)$$

using the conservation of comoving entropy.

We can now introduce the parameter N_{eff} , called the *effective number of relativistic species* [173–175], which accounts for the non-instantaneous decoupling of neutrinos (in which case we would have $N_{\text{eff}} = 3$) and the consequent injection of some energy. For example, the energy density of radiation ρ_r is written as the sum of photons and neutrinos:

$$\rho_r = \left[1 + \frac{7}{8} \left(\frac{4}{11} \right)^{\frac{4}{3}} N_{\text{eff}} \right] \rho_\gamma \quad (8)$$

with $N_{\text{eff}} = 3.044$ [5, 175–179]. Any additional relativistic particle produced before recombination can be treated as an additional contribution to this number (but also

other contributions are possible, for example from inflationary gravitational waves [180]. Therefore, observing a $\Delta N_{\text{eff}} \neq 0$ could be a hint of new physics. Conversely, smaller values suggest a lower-temperature reheating [181] than expected in the Λ CDM Universe.

Notably, since the radiation energy density ρ_r is proportional to the effective number of neutrinos, different values of N_{eff} modify the sound horizon at recombination. In particular, larger values decrease the horizon and, consequently, require higher values of H_0 , potentially shifting towards late-time H_0 measurements. It has been argued that such a shift would exacerbate the tension with large-scale structure data, but if a proper scale is used to quantify the amplitude of matter fluctuations (σ_{12}), then the consistency is restored [182, 183].

The strong correlation with the two *pillars* of the Planck vs. ACT inconsistency—the baryon density $\Omega_b h^2$ and the spectral index n_s [184, 185]—makes N_{eff} an interesting extra parameter to include in this study.

6. Early Dark Energy

Early Dark Energy (EDE) models are a natural hypothesis for dark energy; see, e.g., Refs. [23, 78, 186–214]. Deviating from the traditional cosmological constant framework, EDE models account for a non-negligible contribution from dark energy in the early Universe. In addition, these EDE models can be based on generic dark energy fluids that are inhomogeneous. Their density and pressure vary over time, leading to a non-static equation of state. The phenomenological analyses of these inhomogeneous dark energy models usually require additional dark energy clustering parameters: the dark energy effective sound speed and the dark energy anisotropic stress. The effective sound speed determines the clustering properties of dark energy and consequently affects the growth of matter density fluctuations. Therefore, in principle, its presence could be revealed in large-scale structure observations. The growth of perturbations can also be affected by anisotropic stress contributions, which lead to a damping of velocity perturbations.

Recently, EDE models have garnered significant attention, particularly due to their potential role in addressing some of the aforementioned cosmological tensions [12, 23, 193, 215]. Our analysis will concentrate on the EDE implementation detailed in [201]. This model proposes that, in the early Universe, a light scalar field deviates from its potential minimum and, constrained by Hubble friction, behaves functionally similar to a cosmological constant. As soon as the Hubble parameter falls below the mass of the field at some particular redshift z_* , the scalar field rolls down its potential and begins to oscillate about the minimum. To avoid spoiling late-time cosmology, the vacuum energy must redshift away more quickly than matter (i.e., faster than a^{-3}), and the field should remain a subdominant component. A typical set of parameters used in this model includes the

² We opt for the first one simply because we wanted to impose the most stringent limit on the helium mass fraction to observe a shift in Ω_b .

fractional contribution to the total energy density of the Universe, $f_{\text{EDE}}(z) \equiv \rho_{\text{EDE}}(z)/\rho_{\text{tot}}(z)$, evaluated at the critical redshift z_c where it reaches its maximum value, and θ_i , which typically describes the initial field displacement. This particular behavior implies a larger amount of energy density in the early Universe (just prior to recombination), a reduction of the sound horizon, and, consequently, a larger value of the Hubble constant inferred from CMB observations. This is why EDE models have been proposed as a possible solution to the Hubble constant tension.

From observations of the primary temperature anisotropies of the CMB with Planck data, there is no evidence for an EDE scenario ($f_{\text{EDE}} < 0.087$ at 95% CL [201]) regardless of the likelihood used [216]. However, ACT data show a mild preference for nonzero EDE ($f_{\text{EDE}} = 0.142^{+0.039}_{-0.072}$ at 68% CL [86]) [86, 87, 217].

III. STATISTICS

Given a set of parameters θ defining a certain underlying theoretical model \mathcal{M} , and the observed data d , we can apply *Bayes' Theorem* [218–220]:

$$p(\theta|d) = \frac{p(d|\theta)p(\theta)}{p(d)}. \quad (9)$$

In Eq. (9), $p(\theta|d)$ is the *posterior* probability, which represents our degree of belief about the parameters θ after observing d . The term $p(d|\theta)$, also called the *likelihood* $\mathcal{L}(\theta)$, is the 'probability'³ of observing the data given the parameters. The factor $p(\theta)$ is called the *prior* and represents all the information we have about the parameters before observing the data; it is common in the literature to choose a flat prior.⁴ If this is the case, the posterior becomes functionally identical to the likelihood up to a proportionality constant. On the other hand, any prior knowledge about the parameters is reflected in the posterior. As a consequence, the best parameters of the model are usually those that maximize the posterior, following the *Maximum a Posteriori* (MAP) method, where θ_{MP} satisfies $\partial p(\theta|d)/\partial\theta = 0$. This contrasts with the *Maximum Likelihood* (ML) method, which finds parameters that maximize the likelihood. For flat, uninformative priors, MAP and ML are identical [221, 222]. Because the posterior is a probability distribution of the parameters, we need a normalization factor, $p(d)$, in Eq. (9). It is defined as

$$\frac{\int p(d|\theta)p(\theta)d\theta}{p(d)} = 1 \longrightarrow \int p(d|\theta)p(\theta)d\theta = p(d). \quad (10)$$

³ The likelihood is not a probability distribution over θ , but rather a function of θ given the observed data [219].

⁴ It should be noted that even though we assign a flat prior to a parameter θ , the prior on a function $f(\theta)$ becomes informative.

This term is also called the *Bayesian evidence*. As we will see, it is an important tool for quantifying model performance.

Bayesian Evidence

When comparing models, it is important to take into account the volume of the parameter space and, for example, penalize models with parameters that are unconstrained by the data—an issue that may stem from observational limitations rather than a flaw in the theory. In fact, the 'performance' of a model in fitting the data is highly correlated with its complexity: with a sufficiently high number of parameters, it is possible to accommodate almost any observed data. Therefore, it is crucial to break this correlation by quantifying the necessity for a model not only to fit the data but also to ensure that all parameters are "essential." This principle is encapsulated in the phrase *Pluralitas non est ponenda sine necessitate*,⁵ or, in other words, the simplest theory compatible with the available evidence ought to be preferred. This is known as the *Occam's razor principle*.

In statistical terms, a cosmological model \mathcal{M} is simply the combination of a set of parameters θ and their prior distribution, $p(\theta|\mathcal{M})$. With this definition in mind, let us reconsider the Bayesian evidence presented in Eq. (10) [219, 220]:

$$p(d|\mathcal{M}) \equiv \int_{\Omega_{\mathcal{M}}} p(d|\theta, \mathcal{M})p(\theta|\mathcal{M})d\theta, \quad (11)$$

where we have explicitly included the model conditionality. The Bayesian evidence in Eq. (11) is the average of the likelihood $p(d|\theta, \mathcal{M})$ under the prior for a specific model choice. Specifically, it accounts for how well the parameters fit the data while also incorporating information about the change in parameter volume from the prior to the posterior [223]. Moreover, adding more parameters penalizes the evidence, in accordance with Occam's razor, ensuring that unconstrained parameters do not contribute, as desired.

A. Bayes Factor

If we have two different models, \mathcal{M}_0 and \mathcal{M}_1 , and we want to check whether \mathcal{M}_1 better describes the data, we can use Bayes' theorem Eq. (9), assigning a prior to each model, and introduce the *Bayes factor* [224, 225]:

$$\frac{p(\mathcal{M}_0|d)}{p(\mathcal{M}_1|d)} = \frac{p(d|\mathcal{M}_0)}{p(d|\mathcal{M}_1)} \frac{p(\mathcal{M}_0)}{p(\mathcal{M}_1)} = B_{01} \frac{p(\mathcal{M}_0)}{p(\mathcal{M}_1)}. \quad (12)$$

⁵ Attributed to the Franciscan monk William of Ockham (ca. 1285–1349).

In most cases, we do not favor any model, so $p(\mathcal{M}_0) = p(\mathcal{M}_1)$. If a parameter θ_i is poorly constrained, then when it varies, the likelihood in Eq. (11) is approximately constant in the integral. If the prior is factorizable (which is true in almost all cases), the integral decouples and evaluates to unity, meaning it does not contribute to the evidence and consequently to the Bayes factor B in Eq. (12). This ensures that unconstrained parameters are rightly attributed to poor measurements rather than penalizing the model.

If the Bayes factor B_{01} is greater than one, it suggests that the original model is favored, and we should not switch to \mathcal{M}_1 . On the other hand, if it is smaller than one, we have no evidence to favor \mathcal{M}_0 over \mathcal{M}_1 . To better quantify the strength of the evidence, we can use the modified [220] Jeffreys' scale [226] and compare the Bayes factor with the following thresholds:

- $|\ln B_{01}| < 1$ is ranked as *inconclusive*, and \mathcal{M}_0 has a posterior probability < 0.750.
- $1 \leq |\ln B_{01}| < 2.5$ is ranked as *weak*, and \mathcal{M}_0 has a posterior probability of 0.750.
- $2.5 \leq |\ln B_{01}| < 5$ is ranked as *moderate*, and \mathcal{M}_0 has a posterior probability of 0.923.
- $|\ln B_{01}| \geq 5$ is ranked as *strong*, and \mathcal{M}_0 has a posterior probability of 0.993.

If we take two models, \mathcal{M}_0 and \mathcal{M}_1 , that predict the same value for the parameters θ , then \mathcal{M}_1 is preferred only if the parameters are strongly constrained by the data due to the integration over the entire prior volume in the Bayesian evidence. In other words, the Bayes factor also measures how the fit performs given the priors (it has a likelihood that is less informative than the prior) [220].

B. Suspiciousness

Suppose now that we fix a specific model \mathcal{M} and that the data come from two independent datasets, A and B .⁶ If A is described by a set of parameters θ_A and B by θ_B , then the total evidence can be written as the product of the individual evidences (because the likelihood, but not the posterior, factorizes). Therefore, we can test the confidence in the ability to combine the datasets using the *robustness* [90, 225, 227]:

$$R = \frac{p(A, B)}{p(A)p(B)} \quad (13)$$

where $p(A, B) = \int p(A|\theta)p(B|\theta)p(\theta)d\theta$, omitting the conditionality to the model for simplicity. The numerator represents the case where both datasets are explained

by the same parameters within the model, while the denominator allows each dataset to be explained by different parameters. The robustness is a ratio of evidences, similar to the Bayes factor Eq. (12), but applied within a specific model to test the compatibility between datasets. Therefore, the same considerations apply [90]. If $R \gg 1$ ($R \ll 1$), we can interpret it as both datasets being consistent (inconsistent).⁷ R is strongly prior-dependent for shared parameters that are constrained; in fact, narrowing the priors decreases the value of R . Hence, it must be handled with great care, as an ill-defined prior can indicate an agreement between two datasets that are not actually compatible.⁸ For a better interpretation of R [90, 227, 228], we can use the definition of conditional probability and express it as $R = p(A|B)/p(A)$. Thus, we can say that R represents the relative confidence we have in dataset A given knowledge of B , compared to the confidence in A alone. From this perspective, it is straightforward that $R > 1$ means that B strengthens our confidence in A .

If we take the logarithm of Eq. (13), we obtain

$$\log S = \log R - \log I \quad (14)$$

where S is the *Suspiciousness* [90, 229], and I is the *Information ratio*. The quantity I accounts for the proportionality of the prior and is defined as $\log I = \mathcal{D}_A + \mathcal{D}_B - \mathcal{D}_{AB}$, where \mathcal{D} represents the Kullback-Leibler divergence [230–234]. Hence, S is prior-independent [235] and depends only on the actual mismatch between the posteriors. It is an extremely useful tool for testing the degree of inconsistency between two datasets under different extensions to the standard model, eliminating any possible bias due to prior volume effects [90].

If the posteriors are such that we may approximate them with a Gaussian (in a broader sense [90, 235]), with means and covariance matrices μ and σ , then the suspiciousness follows the χ^2_d distribution, where d is the effective number of degrees of freedom constrained by both datasets [74, 75, 90, 222]:

$$\log S = \frac{d}{2} - \frac{\chi^2}{2} \quad (15)$$

with

$$\chi^2 = (\mu_A - \mu_B)^T (\sigma_A + \sigma_B)^{-1} (\mu_A - \mu_B). \quad (16)$$

For an easier interpretation of the result, we can use the inverse cumulative χ^2 distribution to obtain the tension probability:

$$p = \int_{\chi^2}^{\infty} \frac{x^{d/2-1} e^{-x/2}}{2^{d/2} \Gamma(d/2)} dx. \quad (17)$$

⁷ If the datasets are not compatible with one another, since only the likelihoods can be multiplied, we should not expect $R = 1$ in this scenario.

⁸ However, the reverse is not possible due to the unidirectional increase of volume effects.

⁶ New parameters may be introduced when combining independent datasets due to new nuisance parameters or increased constraining power.

The tension level is then given by

$$\sigma(p) = \sqrt{2} \operatorname{erfc}^{-1}(1 - p), \quad (18)$$

which represents the relationship between a given cumulative probability p and its corresponding number of standard deviations σ in a normal distribution. Thus, a 3σ deviation corresponds to $p < 0.3\%$, indicating strong tension. The tension probability quantifies the likelihood that the observed tension occurs by chance.

C. Goodness-of-fit

If we want to understand how *strong* the compromise is when joining two datasets instead of considering them independently, we need to perform the *goodness-of-fit* test [228, 235]. This test evaluates the cost of explaining datasets with the same parameter values and is quantified by the estimator:

$$Q_{\text{DMAP}}^2 = 2 \ln \mathcal{L}_A(\hat{\theta}_A) + 2 \ln \mathcal{L}_B(\hat{\theta}_B) - 2 \ln \mathcal{L}_{A+B}(\hat{\theta}_{AB}) \quad (19)$$

Here, $\hat{\theta}_A$ denotes the parameter values that “best” describe dataset A . In frequentist statistics, the parameters are taken such that $\hat{\theta} \equiv \theta_{ML}$, and therefore, $Q_{\text{DMAP}} \equiv \sqrt{\chi^2}$. On the other hand, in the context of Bayesian analysis, $\hat{\theta} \equiv \theta_{\text{MAP}}$. As we have seen, for flat priors, these two cases are identical. The test statistic Q_{DMAP} is widely used in cosmology (see, e.g., [21, 208, 235]). When the likelihoods and posteriors are Gaussian, Q_{DMAP}^2 follows a χ^2 distribution [228, 235]. The goodness-of-fit is expected to degrade by one for each measured parameter and indicates tension if the decrease is significantly higher. Only parameters that are constrained by the data over the prior can contribute to a tension, as prior-constrained parameters cannot be optimized to improve the data fit.

D. AIC

To complete the set of statistical metrics used in this paper, we include the simplest and most widely used Akaike Information Criterion (AIC) [236] (e.g., in [237–243]). The reason for employing this criterion is to facilitate comparisons with results already available in the literature.

AIC allows for direct and straightforward model comparison, providing a refinement beyond a simple χ^2 difference. As seen from its definition:

$$\text{AIC} = \chi^2 + 2n_p, \quad (20)$$

it accounts for the number of fitting parameters (n_p). Therefore, it not only evaluates the quality of the fit but also penalizes extra model parameters. We compare the AIC values of non-standard models to that of ΛCDM

Parameter	Prior
$\Omega_b h^2$	[0.005, 0.1]
$\Omega_c h^2$	[0.001, 0.99]
$100 \theta_{\text{MC}}$	[0.5, 10]
τ	[0.004, 0.8]
$\log(10^{10} A_S)$	[1.61, 3.91]
n_s	[0.8, 1.2]
α_s	[-1, 1]
w	[-3, 1]
Ω_k	[-0.4, 0.4]
Y_p	[0.1, 0.3]
N_{eff}	[1, 5]
f_{EDE}	[0, 0.5]
θ_i	[0.1, 3.1]
$\log_{10} z_c$	[3.1, 4.3]

Table I: List of the parameter priors used in the MCMC.

by computing the difference $\Delta\text{AIC} = \text{AIC}_{\Lambda\text{CDM}} - \text{AIC}_i$, using the standard model as the benchmark. A positive ΔAIC indicates a preference for the non-standard model. More concretely, we quantify this preference using standard thresholds:

- If $0 \leq \Delta\text{AIC} < 2$, there is *weak evidence* in favor of the new model i compared to the standard model.
- If $2 \leq \Delta\text{AIC} < 6$, this is considered *positive evidence*.
- If $6 \leq \Delta\text{AIC} < 10$, we classify it as *strong evidence*.
- If $\Delta\text{AIC} > 10$, there is *very strong evidence* supporting model i against ΛCDM .

IV. METHODS AND DATASET

To assess the inconsistency between Planck and ACT, as well as to evaluate the sensitivity of the Hubble tension in different scenarios, we make use of three different datasets:

- Planck CMB temperature and polarization power spectra from the legacy Planck release [5, 244] (henceforth Planck). Specifically, we use the combination of the **Commander** likelihood for temperature TT data at low multipoles ($2 \leq \ell \leq 29$), the **SimAll** likelihood for the same range but with polarization EE, and the **Plik** high-multipole likelihood for temperature TT, polarization EE, and cross-spectra TE at high multipoles ($30 \leq \ell \leq 2508$).

- SH0ES collaboration calibration of the Hubble constant ($H_0 = 73 \pm 1 \text{ km s}^{-1} \text{ Mpc}^{-1}$) using the three-rung distance ladder method with Cepheids [245].
- ACT DR4 [6] + τ prior ($\mu = 0.06$, $\sigma_\tau = 0.01$ [7]).

For all cosmological parameters, we choose flat-prior distributions, varying them uniformly within the conservative ranges listed in Tab. I, except for the optical depth, for which we set a Gaussian prior when the dataset in consideration is ACT (as stated above) and when we consider the extension $\Lambda\text{CDM+BBN}$, where BBN refers to the BBN prior on Y_p , as explained in Sec. II 4.

For each model, we perform Monte Carlo Markov Chain (MCMC) analyses using the publicly available package `Cobaya` [246], computing the theoretical predictions with `CAMB` [247–250] and a modified version of `CLASS` [251, 252] for EDE [201].⁹ We explore the posteriors of our parameter space using the MCMC sampler developed for `CosmoMC` [253], tailored for parameter spaces with a speed hierarchy, which also implements the “fast dragging” procedure [254]. The convergence of the chains obtained with this procedure is tested using the Gelman-Rubin criterion [255], with a threshold for chain convergence of $R - 1 \lesssim 0.02$.

Regarding the computation of the AIC and the goodness-of-fit, we used the minimum χ^2 obtained with the `py-BODYQA` minimizer [256–258]. In light of the H_0 tension, in Eq. (19), we replace dataset B with the SH0ES dataset and assume $\chi_B^2 = 0$ [21]. For the Bayes factor, we computed the Bayesian evidence using the publicly available code `MCEvidence`¹⁰ [259], assigning to \mathcal{M}_0 in Eq. (12) the model with the lowest evidence.

To compute the suspiciousness in Eq. (15), we assumed uncorrelated datasets. This is not strictly the case for ACT and Planck since, despite being two independent measurements, their multipole ranges overlap. To properly analyze any potential tension between the two, one should follow [229]. However, no joint likelihood exists for these two datasets. Although this approach offers only approximate results, it allows us to assess inconsistencies between the datasets and how they change across different models, without introducing any bias due to prior volume effects.

V. RESULTS

In Tab. II, the constraints on the parameters beyond the standard model are reported. In Tab. III and Fig. 1, the estimates for the spectral index n_s can be found, whereas in Tab. IV and Fig. 2, those for $\Omega_b h^2$ are presented. To analyze the performance of a model with respect to the others, given a dataset combination, we can

study the χ^2 and ΔAIC values in Fig. 3, Fig. 4, and Tab. V. For further comparison, the Bayes factors are reported in Fig. 5. To assess the Planck and ACT discrepancy, the tension levels are depicted in Fig. 6, and all Suspiciousness parameters are reported in Tab. VI. Lastly, to evaluate the sensitivity of the Hubble tension to the underlying cosmology, we examine the Q_{DMAP} values in Tab. VII and Fig. 7.

Before analyzing the performance of each model separately, we first present a general overview of model performance according to the Bayes factor defined in Eq. (12). As anticipated in Sec. IV, zero values correspond to the cases with the lowest Bayesian evidence ($B_{00} = 0$). For Planck-only data, $\Lambda\text{CDM}+\Omega_k$ is the model favored by the data. Only the Helium-fraction alternative (both with and without the BBN prior) yields a Bayes factor indicative of a *moderate* preference for \mathcal{M}_0 over \mathcal{M}_1 . In every other extension, the evidence strongly supports Ω_k , with a posterior probability exceeding 99.3%. If we include SH0ES data, the non-flat geometry is strongly disfavored, as are all the other alternatives, in favor of the EDE scenario. This result is expected, as EDE was introduced to address the Hubble tension. Notably, imposing an HZ spectrum generally worsens the Bayesian factor for most models, although EDE with Planck alone experiences a slight improvement.

In the case of ACT-only data, we observe smaller overall Bayes factors but still see no clear *weak* or *moderate* preferences, except in a few instances. Imposing $n_s = 1$ consistently reduces the evidence for most extensions, with the following exceptions:

$$\begin{aligned} |\ln B_{01}| &= 10.04 \xrightarrow{n_s=1} 11.04 & (\Lambda\text{CDM}+Y_p) \\ |\ln B_{01}| &= 10.37 \xrightarrow{n_s=1} 12.27 & (\Lambda\text{CDM}+\text{BBN}) \\ |\ln B_{01}| &= 11.42 \xrightarrow{n_s=1} 11.65 & (\Lambda\text{CDM}+N_{\text{eff}}) \end{aligned}$$

for ACT+SH0ES. ACT-only data are insufficient to decisively distinguish among the extensions with Y_p , $Y_p+\text{BBN}$ prior, and Ω_k , all combined with $n_s = 1$. Again, the inclusion of SH0ES amplifies the preference for EDE, as EDE+ $n_s = 1$ is now the preferred model according to the data, with only a *weak* preference against EDE alone, while all other alternatives remain strongly disfavored.

If we now look at Fig. 1, it is immediately apparent that Planck constraints on n_s remain unaffected, but the set of $\{\alpha_s, Y_p, N_{\text{eff}}, \text{EDE}\}$ alternatives shifts ACT values and increases error bars, allowing an observational consistency below 2σ . Specifically, we have $n_s = 0.981 \pm 0.020$, $n_s = 0.977 \pm 0.028$, $n_s = 0.961 \pm 0.034$ and $n_s = 0.994^{+0.039}_{-0.046}$ at 68% CL for each respective model. The inclusion of SH0ES increases the expectation values for both Planck and ACT and enhances their overlap, with the exception of EDE. On the other hand, the baryon parameter is less sensitive to the different models, and an agreement is almost never recovered. The HZ spectrum does increase the $\Omega_b h^2$ value for both ACT and Planck;

⁹  CLASS EDE

¹⁰  MCEvidence

Extra-parameter	α_s	w	Ω_k	Y_p	N_{eff}	f_{EDE}
Planck						
n_s free	-0.0060 ± 0.0067	$-1.58^{+0.25}_{-0.32}$	-0.045 ± 0.018	0.240 ± 0.013	$2.97^{+0.21}_{-0.19}$	< 0.0866
$n_s = 1$	0.0103 ± 0.0067	$-1.50^{+0.16}_{-0.21}$	$-0.096^{+0.026}_{-0.023}$	0.2929 ± 0.0074	3.71 ± 0.11	0.135 ± 0.020
Planck + SH0ES						
n_s free	-0.0047 ± 0.0068	-1.193 ± 0.040	0.0088 ± 0.0020	0.258 ± 0.013	3.48 ± 0.13	0.116 ± 0.025
$n_s = 1$	0.0092 ± 0.0066	-1.064 ± 0.030	0.0011 ± 0.0019	0.2898 ± 0.0073	3.71 ± 0.10	0.139 ± 0.019
ACT						
n_s free	0.060 ± 0.028	-1.16 ± 0.42	$-0.003^{+0.020}_{-0.017}$	0.205 ± 0.031	2.36 ± 0.43	$0.148^{+0.057}_{-0.094}$
$n_s = 1$	0.043 ± 0.022	-1.18 ± 0.43	$0.001^{+0.017}_{-0.015}$	0.226 ± 0.017	2.81 ± 0.21	$0.120^{+0.054}_{-0.078}$
ACT + SH0ES						
n_s free	0.063 ± 0.028	-1.161 ± 0.063	0.0102 ± 0.0039	0.242 ± 0.029	3.44 ± 0.23	0.123 ± 0.031
$n_s = 1$	0.060 ± 0.021	-1.174 ± 0.062	0.0109 ± 0.0034	0.220 ± 0.017	3.17 ± 0.18	0.106 ± 0.027

Table II: Best-fit parameter values at 68% CL for different datasets, with and without imposing an HZ spectrum. The upper bounds are given at 95% CL. These constraints apply to the extra parameter for each alternative model proposed in this paper. Regarding EDE, we report only f_{EDE} , as it is better constrained and more indicative of the impact of EDE compared to $\log_{10} z_c$ and θ_i .

Model	Planck	Planck+SH0ES	ACT	ACT+SH0ES
ΛCDM	0.9649 ± 0.0044	0.9732 ± 0.0040	1.008 ± 0.015	1.025 ± 0.015
$\Lambda\text{CDM} + \alpha_s$	0.9633 ± 0.0047	0.9721 ± 0.0044	0.981 ± 0.020	0.996 ± 0.019
$w\text{CDM}$	0.9654 ± 0.0043	0.9649 ± 0.0043	1.007 ± 0.016	1.009 ± 0.016
$\Lambda\text{CDM} + \Omega_k$	0.9701 ± 0.0048	0.9649 ± 0.0042	1.009 ± 0.017	1.004 ± 0.016
$\Lambda\text{CDM} + Y_p$	0.9619 ± 0.0070	0.9774 ± 0.0065	0.977 ± 0.028	1.023 ± 0.026
$\Lambda\text{CDM} + \text{BBN}$	0.9637 ± 0.0047	0.9725 ± 0.0043	1.007 ± 0.016	1.024 ± 0.015
$\Lambda\text{CDM} + N_{\text{eff}}$	0.9610 ± 0.0085	0.9843 ± 0.0053	0.961 ± 0.034	1.041 ± 0.017
EDE	$0.9693^{+0.0069}_{-0.0082}$	0.9902 ± 0.0060	$0.994^{+0.039}_{-0.046}$	0.985 ± 0.032

Table III: Constraints on n_s at 68% CL for the various extensions of the standard model considered in this paper.

however, the excursion for ACT is not comparable to that of Planck, thus exacerbating this parameter tension.

1. ΛCDM

From previous work (see, e.g., [74, 75, 91]), it is known that within the standard cosmological model, there is a $\sim 2.6\sigma$ tension level (see Eq. (18)) between Planck and ACT measurements. This level serves as a benchmark for all other cosmological scenarios considered here: if the Planck–ACT agreement for a given extension lies below this threshold, the model appears promising for alleviating the tension. Adding the SH0ES prior exacerbates the tension to more than 3σ , as seen in Fig. 6. If we reduce the number of free parameters, i.e., fix n_s to unity, the

results are inverted. In fact,

$$\log S = -5.33 \xrightarrow{n_s=1} -7.09 \quad (\text{Planck})$$

$$\log S = -8.63 \xrightarrow{n_s=1} -5.15 \quad (\text{Planck+SH0ES})$$

Since ΛCDM is, by definition, not suitable for solving the Hubble tension, we adopt its $Q_{\text{DMAP}}^{\Lambda}$ value as our reference: $Q_{\text{DMAP}}^{\Lambda} = 5.31$ for Planck-only analyses. This value can decrease when additional datasets are incorporated (see, e.g., [21]). Replacing Planck with ACT data yields a smaller tension, with $Q_{\text{DMAP}}^{\Lambda} = 3.47$, signifying a comparatively moderate discrepancy. Of particular interest is the role of the HZ spectrum: it substantially lowers the discrepancy for Planck, yet slightly increases it for ACT. Specifically,

$$Q_{\text{DMAP}} = 5.31 \xrightarrow{n_s=1} 2.81 \quad (\text{Planck})$$

$$Q_{\text{DMAP}} = 3.47 \xrightarrow{n_s=1} 3.84 \quad (\text{ACT})$$

Model	Planck	Planck+SH0ES	ACT	ACT+SH0ES
n_s free				
ΛCDM	0.02236 ± 0.00015	0.02264 ± 0.00014	0.02152 ± 0.00030	0.02171 ± 0.00030
$\Lambda\text{CDM} + \alpha_s$	0.02240 ± 0.00016	0.02267 ± 0.00015	0.02137 ± 0.00032	0.02156 ± 0.00032
$w\text{CDM}$	0.02240 ± 0.00015	0.02237 ± 0.00015	0.02151 ± 0.00030	0.02153 ± 0.00031
$\Lambda\text{CDM} + \Omega_k$	0.02258 ± 0.00017	0.02236 ± 0.00015	0.02149 ± 0.00032	0.02151 ± 0.00032
$\Lambda\text{CDM} + Y_p$	0.02229 ± 0.00021	0.02273 ± 0.00019	0.02111 ± 0.00042	0.02169 ± 0.00041
$\Lambda\text{CDM} + \text{BBN}$	0.02233 ± 0.00015	0.02262 ± 0.00014	0.02150 ± 0.00031	0.02169 ± 0.00030
$\Lambda\text{CDM} + N_{\text{eff}}$	0.02227 ± 0.00022	0.02283 ± 0.00015	0.02098 ± 0.00046	0.02185 ± 0.00032
EDE	0.02248 ± 0.00021	0.02283 ± 0.00021	$0.02150^{+0.00057}_{-0.00063}$	0.02143 ± 0.00045
$n_s = 1$				
ΛCDM	0.02294 ± 0.00014	0.02300 ± 0.00014	0.02159 ± 0.00029	0.02169 ± 0.00041
$\Lambda\text{CDM} + \alpha_s$	0.02283 ± 0.00016	0.02292 ± 0.00015	0.02133 ± 0.00031	0.02155 ± 0.00039
$w\text{CDM}$	0.02296 ± 0.00014	0.02293 ± 0.00014	0.02158 ± 0.00029	0.02169 ± 0.00030
$\Lambda\text{CDM} + \Omega_k$	0.02321 ± 0.00015	0.02297 ± 0.00014	0.02154 ± 0.00030	0.02198 ± 0.00026
$\Lambda\text{CDM} + Y_p$	0.02310 ± 0.00014	0.02318 ± 0.00014	0.02125 ± 0.00039	0.02155 ± 0.00039
$\Lambda\text{CDM} + \text{BBN}$	0.02295 ± 0.00014	0.02301 ± 0.00014	0.02156 ± 0.00028	0.02209 ± 0.00030
$\Lambda\text{CDM} + N_{\text{eff}}$	0.02308 ± 0.00014	0.02308 ± 0.00013	0.02126 ± 0.00040	0.02143 ± 0.00045
EDE	0.02302 ± 0.00019	0.02300 ± 0.00019	0.02157 ± 0.00045	0.02155 ± 0.00039

Table IV: Constraints on $\Omega_b h^2$ at 68% CL for the various extensions of the standard model considered in this paper.

Imposing an HZ spectrum appears to mitigate the tension in Planck, while no similar behavior is observed in ACT. Results are shown in Fig. 7 and reported in Tab. VII.

However, even though fixing n_s is a promising approach for reconciling Planck and SH0ES, it is strongly disfavored by ΔAIC , while no significant penalty is given when using ACT-only data. However, once SH0ES is included, the Akaike criterion favors the standard model over the HZ counterpart. The variation in AIC (see Eq. (20)) is:

$$\begin{aligned}\Delta\text{AIC} &= -59.08 \xrightarrow{+SH0ES} -38.76 \quad (\text{Planck}) \\ \Delta\text{AIC} &= -0.06 \xrightarrow{+SH0ES} -2.77 \quad (\text{ACT})\end{aligned}$$

2. $\Lambda\text{CDM} + \alpha_s$

Introducing a scale dependency to the spectral index does not alleviate the Planck-ACT tension. In fact, for all four combinations (with or without SH0ES, and with or without a fixed n_s), the suspiciousness $\log S$ decreases, reaching its most negative value, $\log S = -9.44$, when n_s is free and SH0ES is included; this corresponds to a

tension probability of 0.053%.

Although a running spectral index can slightly reduce the tension with SH0ES relative to ΛCDM , it is not the best model to tackle this tension. However, imposing $n_s = 1$ promotes this scenario to the second-best solution to the Hubble tension for Planck and also yields a moderate reduction in tension for ACT. In particular, we have

$$\begin{aligned}Q_{\text{DMAP}} &= 4.92 \xrightarrow{n_s=1} 2.05 \quad (\text{Planck}) \\ Q_{\text{DMAP}} &= 2.70 \xrightarrow{n_s=1} 2.52 \quad (\text{ACT})\end{aligned}$$

Regarding AIC, α_s is only weakly preferred when fitting ACT data alone ($\Delta\text{AIC} = 1.30$) or Planck+SH0ES ($\Delta\text{AIC} = 0.94$), but becomes strongly favored once SH0ES is included ($\Delta\text{AIC} = 6.01$) and disfavored for Planck-only data ($\Delta\text{AIC} = -3.05$). When n_s is held fixed, the model's performance is nearly identical to ΛCDM for both Planck cases, as seen in Tab. V. In contrast, ACT+SH0ES yields strong support for running, similar to the free- n_s case.

By looking at Tab. II, we notice that across all datasets, the parameter α_s remains consistent with zero at 1σ for Planck, regardless of whether n_s is allowed to

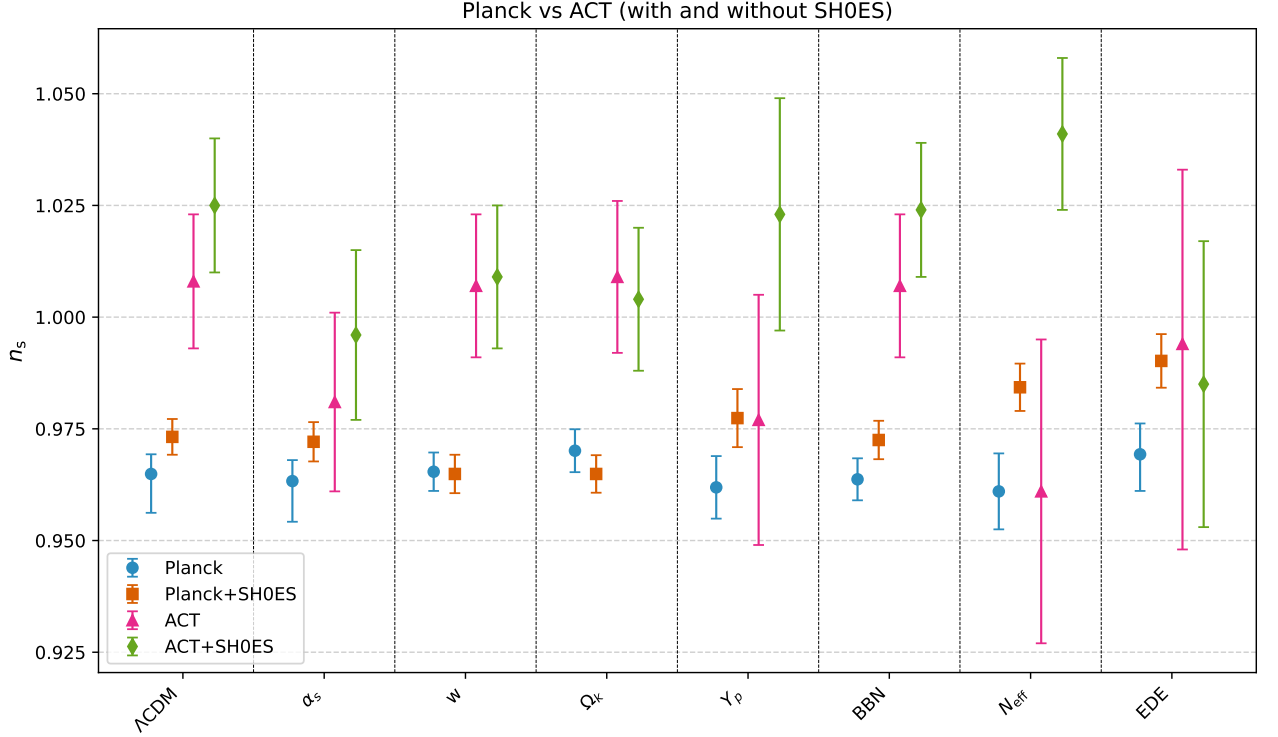


Figure 1: Constraints on n_s at 68% CL for Λ CDM and its extensions. The constraints are given for Planck and ACT alone, as well as in combination with SH0ES.

Model	Planck	Planck+SH0ES	ACT	ACT+SH0ES
n_s free				
Λ CDM + α_s	-3.05	0.94	1.30	6.01
w CDM	-1.60	24.86	-4.71	7.29
Λ CDM + Ω_k	7.65	19.15	-1.19	10.28
Λ CDM + Y_p	-2.03	0.63	2.22	-0.82
Λ CDM + BBN	6.05	6.74	7.64	7.66
Λ CDM + N_{eff}	-6.22	3.59	-2.14	-1.53
EDE	-4.48	16.05	1.06	8.41
n_s fixed				
Λ CDM	-59.08	-38.76	-0.06	-2.77
Λ CDM + α_s	-59.21	-35.20	0.42	6.13
w CDM	-57.36	-34.18	-4.83	7.17
Λ CDM + Ω_k	-26.84	-35.33	-1.21	10.34
Λ CDM + Y_p	-28.60	-13.21	1.93	0.37
Λ CDM + BBN	-53.53	-31.98	7.62	4.95
Λ CDM + N_{eff}	-28.34	-3.60	-3.04	-6.91
EDE	-9.03	13.93	-0.92	6.31

Table V: Δ AIC values for various models. The AIC, as defined in Eq. (20), is compared with the Λ CDM case. This means that a positive value favors the given model over the standard one. To quantify the *strength* of the preference, we use the standard intervals, as presented in Sec. III D.

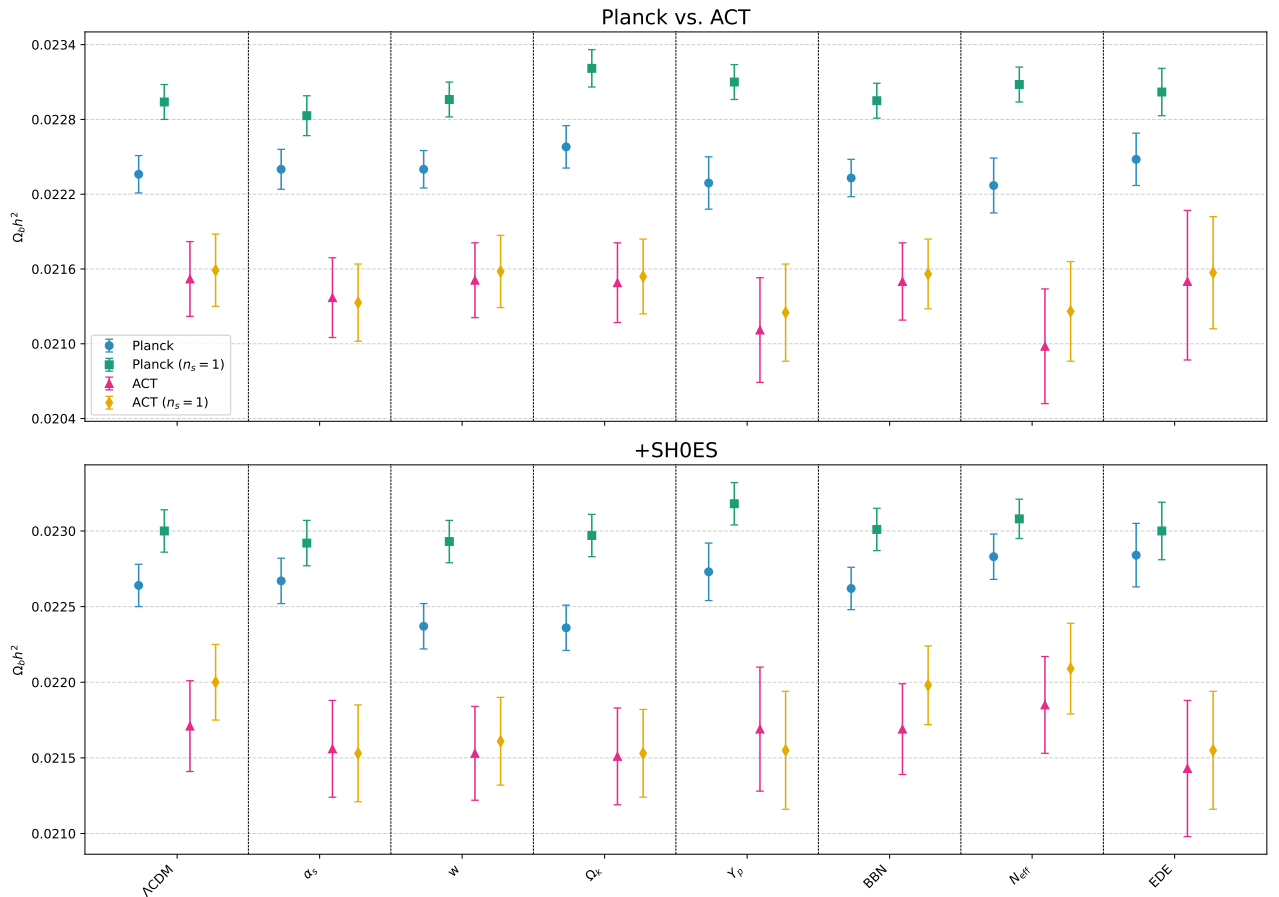


Figure 2: Constraints on $\Omega_b h^2$ at 68% CL for Λ CDM and its extensions. The upper panel shows the constraints for Planck and ACT alone, while the lower panel presents the results when the data are combined with SH0ES.

vary. For the remaining data combinations, $\alpha_s = 0$ is compatible within 2σ .

3. wCDM

Replacing the cosmological constant with a dark energy equation of state w , we increase the number of parameters from 6 to 7. Therefore, despite χ^2 (see Eq. (16)) between the two datasets being larger compared to the standard model ($\chi_w^2 = 17.75$ instead of $\chi_\Lambda^2 = 16.67$), the tension probability is slightly higher: $p = 1.3\%$. When n_s is fixed, w CDM performs poorly at resolving the discrepancy between Planck and ACT, but once SH0ES data are included, the situation changes:

$$\begin{aligned} \log S &= -5.38 \xrightarrow{+SH0ES} -3.95 \quad (n_s \text{ free}) \\ \log S &= -7.05 \xrightarrow{+SH0ES} -3.71 \quad (n_s \text{ fixed}) \end{aligned}$$

Both with and without an HZ spectrum, the tension levels remain at $\sim 2\sigma$, as seen in Fig. 6.

This dark energy alternative offers one of the best scenarios for reconciling CMB and SH0ES measurements.

The Q_{DMAP} values are the lowest for Planck ($Q_{\text{DMAP}} = 1.32$), ACT ($Q_{\text{DMAP}} = 0.17$), and ACT with $n_s = 1$ ($Q_{\text{DMAP}} = 0.18$). The only exception is Planck with a fixed spectral index, which gives the third-lowest value: 2.24.

This model performs best when SH0ES is included, showing very strong ($\Delta^{\text{Planck}}\text{AIC} = 24.86$) and strong ($\Delta^{\text{ACT}}\text{AIC} = 7.29$) evidence against Λ CDM. However, for Planck-only or ACT-only analyses, Λ CDM remains weakly or positively preferred, respectively. Introducing an HZ spectrum preserves the viability of w CDM for ACT and ACT+SH0ES but leads to more negative values for Planck-based datasets:

$$\begin{aligned} \Delta\text{AIC} &= -1.60 \xrightarrow{n_s=1} -57.36 \quad (\text{Planck}) \\ \Delta\text{AIC} &= 24.86 \xrightarrow{n_s=1} -34.18 \quad (\text{Planck+SH0ES}) \end{aligned}$$

For ACT alone with a free spectral index, $w = -1.16 \pm 0.42$ at 68% CL, and with $n_s = 1$, $w = -1.18 \pm 0.43$ at 68% CL; both results are consistent with a cosmological constant, which is recovered when $w = -1$. Meanwhile, Planck+SH0ES excludes $w = -1$ at over 3σ ($w = -1.193 \pm 0.040$), though this significance dimin-

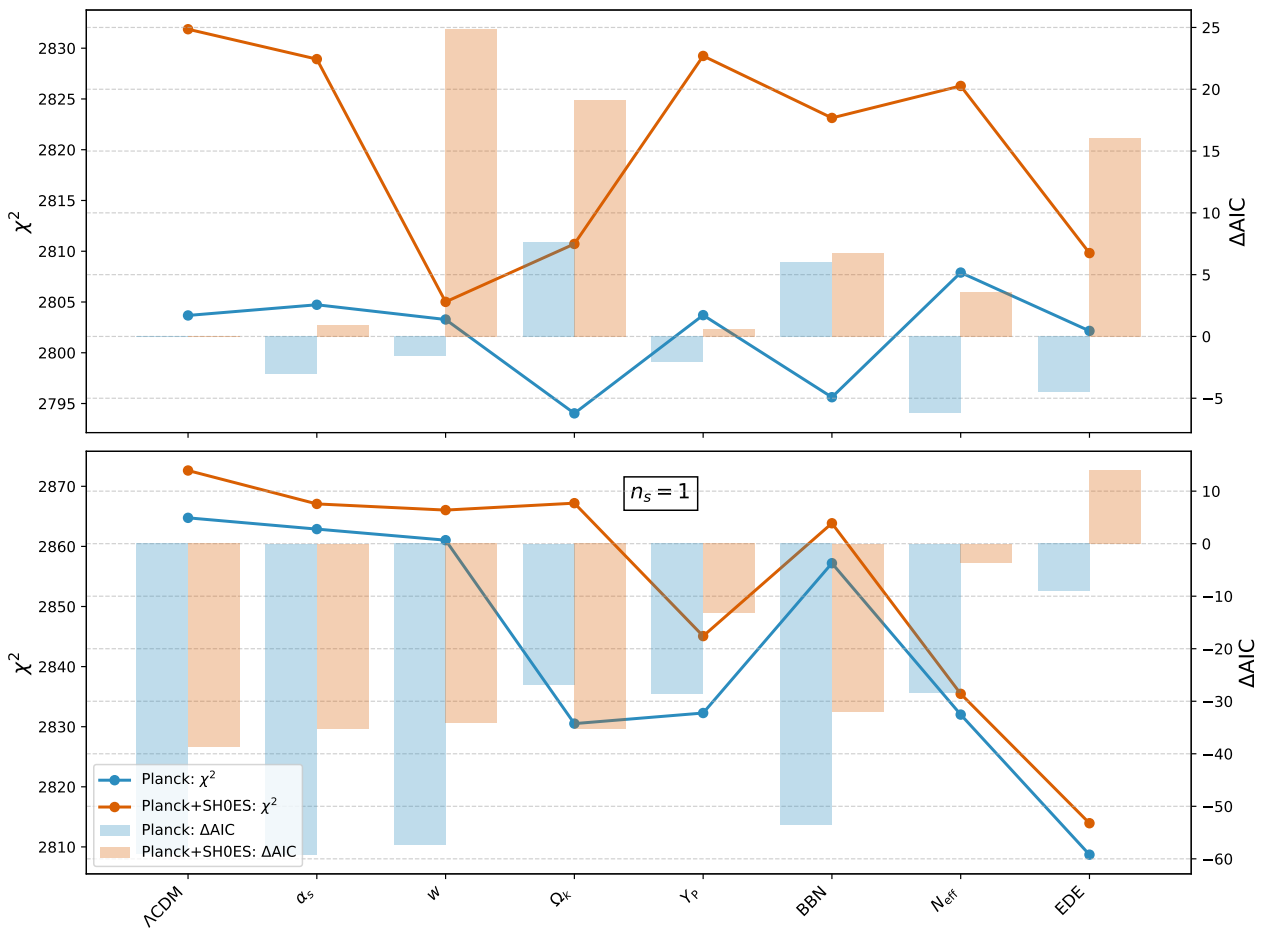


Figure 3: In this graph, the values of χ^2 and ΔAIC are displayed for Planck. The χ^2 values are obtained by minimizing the posterior, as explained in Sec. IV, while the bars represent the difference in AIC between each model and ΛCDM , with AIC computed according to Eq. (20). Since the Akaike criterion accounts for the number of parameters, it is possible to observe that in some cases, even when the χ^2 of a particular extension is lower than the standard value, ΔAIC remains positive, penalizing the model for the increased number of parameters.

ishes to slightly above 2σ ($w = -1.064 \pm 0.030$) under the fixed- n_s assumption.

4. $\Lambda\text{CDM} + \Omega_k$

Although a nonzero curvature appears to be favored by Planck alone (yielding the lowest Bayesian evidence), it does not reconcile the Planck and ACT datasets. This is particularly evident under the HZ assumption, with

$$\log S = -15.12, \sigma(p) = 4.71 \quad (\text{without SH0ES})$$

$$\log S = -8.29, \sigma(p) = 3.31 \quad (\text{with SH0ES})$$

Conversely, if n_s is an extra parameter of the theory, the tension probability more than doubles relative to a flat

universe model, resulting in the second-lowest χ^2 among models with the same number of parameters, and a suspiciousness of $\log S = -5.11$ once SH0ES is included (though it decreases notably if SH0ES is excluded, see Tab. VI).

For Planck, allowing curved geometry slightly reduces the tension with SH0ES ($Q_{\text{DMAP}} = 4.09$), whereas fixing $n_s = 1$ yields the largest discrepancy ($Q_{\text{DMAP}} > 6$). Conversely, for ACT, relaxing flatness lowers the tension substantially (below unity) in both scenarios.

According to the AIC statistics, introducing Ω_k is strongly preferred by Planck and very strongly preferred

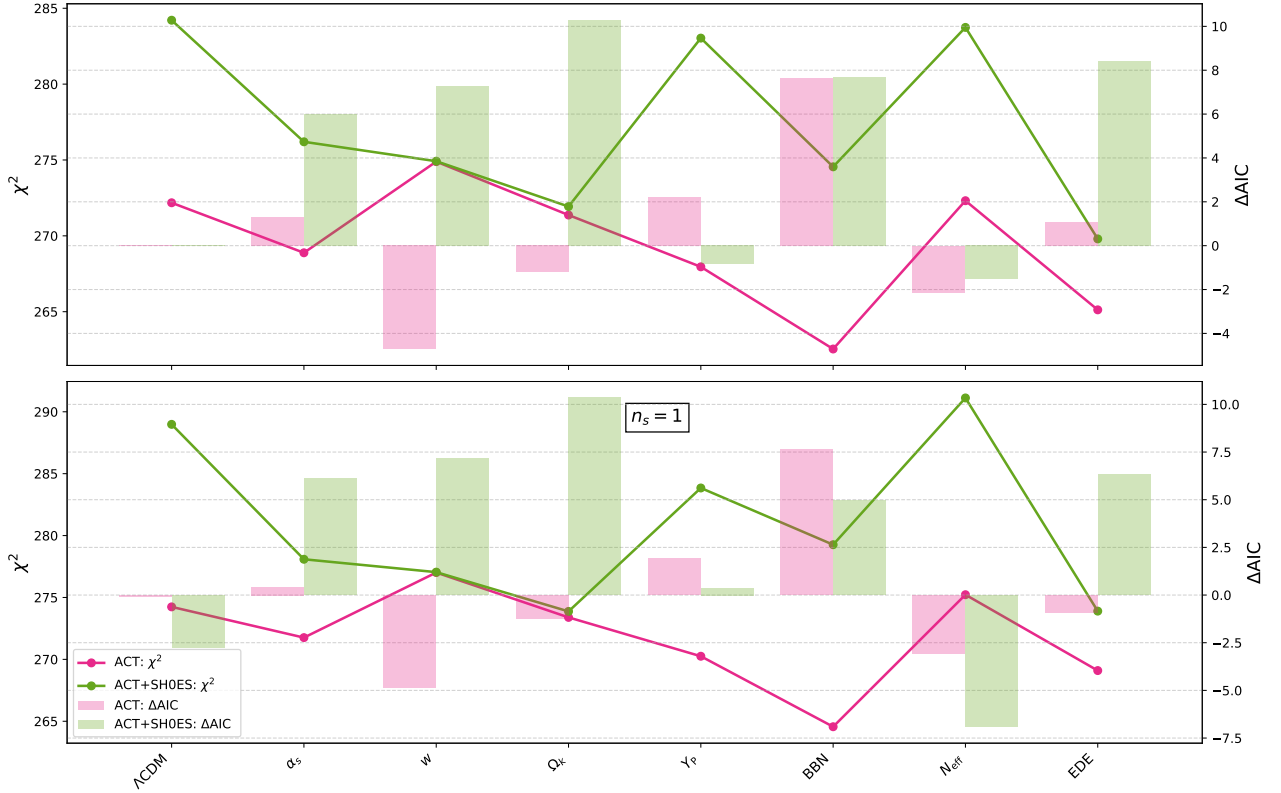


Figure 4: In this graph, the values of χ^2 and ΔAIC are displayed for ACT. The χ^2 values are obtained by minimizing the posterior, as explained in Sec. IV, while the bars represent the difference in AIC between each model and ΛCDM , with AIC computed according to Eq. (20). Since the Akaike criterion accounts for the number of parameters, it is possible to observe that in some cases, even when the χ^2 of a particular extension is lower than the standard value, ΔAIC remains positive, penalizing the model for the increased number of parameters.

by Planck+SH0ES and ACT+SH0ES. Specifically,

$$\begin{aligned} \Delta\text{AIC} &= 7.65 \xrightarrow{+\text{SH0ES}} 19.15 \quad (\text{Planck}) \\ \Delta\text{AIC} &= -1.19 \xrightarrow{+\text{SH0ES}} 10.28 \quad (\text{ACT}). \end{aligned}$$

According to the results in Tab. V, Fig. 3, and Fig. 4, this preference only persists when $n_s = 1$ in the ACT+SH0ES case; elsewhere, it is disfavored.

Planck's constraints on curvature [5] suggest a slight preference for a closed geometry, though consistent with flat space at $\sim 2\sigma$. In contrast, ACT measurements provide tighter bounds on curvature [7], showing perfect compatibility with $\Omega_k = 0$. Including SH0ES data tightens both Planck and ACT posteriors, excluding perfect flatness at over 4σ for Planck and 2σ for ACT. Fixing n_s does not significantly affect the results for ACT. However, Planck alone shifts to $\Omega_k = -0.096^{+0.026}_{-0.023}$ at 68% CL, further increasing the discrepancy with flatness. On the other hand, Planck+SH0ES is now compatible with $\Omega_k = 0$, yielding $\Omega_k = 0.0011 \pm 0.0019$, as reported in

Tab. II.

5. $\Lambda\text{CDM} + Y_p$

Extending ΛCDM by allowing Y_p to vary can yield the second-highest suspiciousness, $\log S \sim 4.6$, in the simple case of free n_s and no SH0ES, largely independent of whether a BBN prior is applied. The same independence to the Helium prior is maintained when SH0ES is included, but it leads to a disfavored tension level ($\sim 3.3\sigma$), similar to the standard ΛCDM one. However, the other two combinations with an HZ spectrum indicate a preference for including the BBN prior:

$$\begin{aligned} \log S &= -9.94 \xrightarrow{+\text{BBN prior}} -8.44 \quad (\text{without SH0ES}) \\ \log S &= -9.10 \xrightarrow{+\text{BBN prior}} -5.54 \quad (\text{with SH0ES}) \end{aligned}$$

In terms of Q_{DMAP} , Planck yields $Q_{\text{DMAP}} = 5.05$ and ACT $Q_{\text{DMAP}} = 3.88$, comparable to the base results.

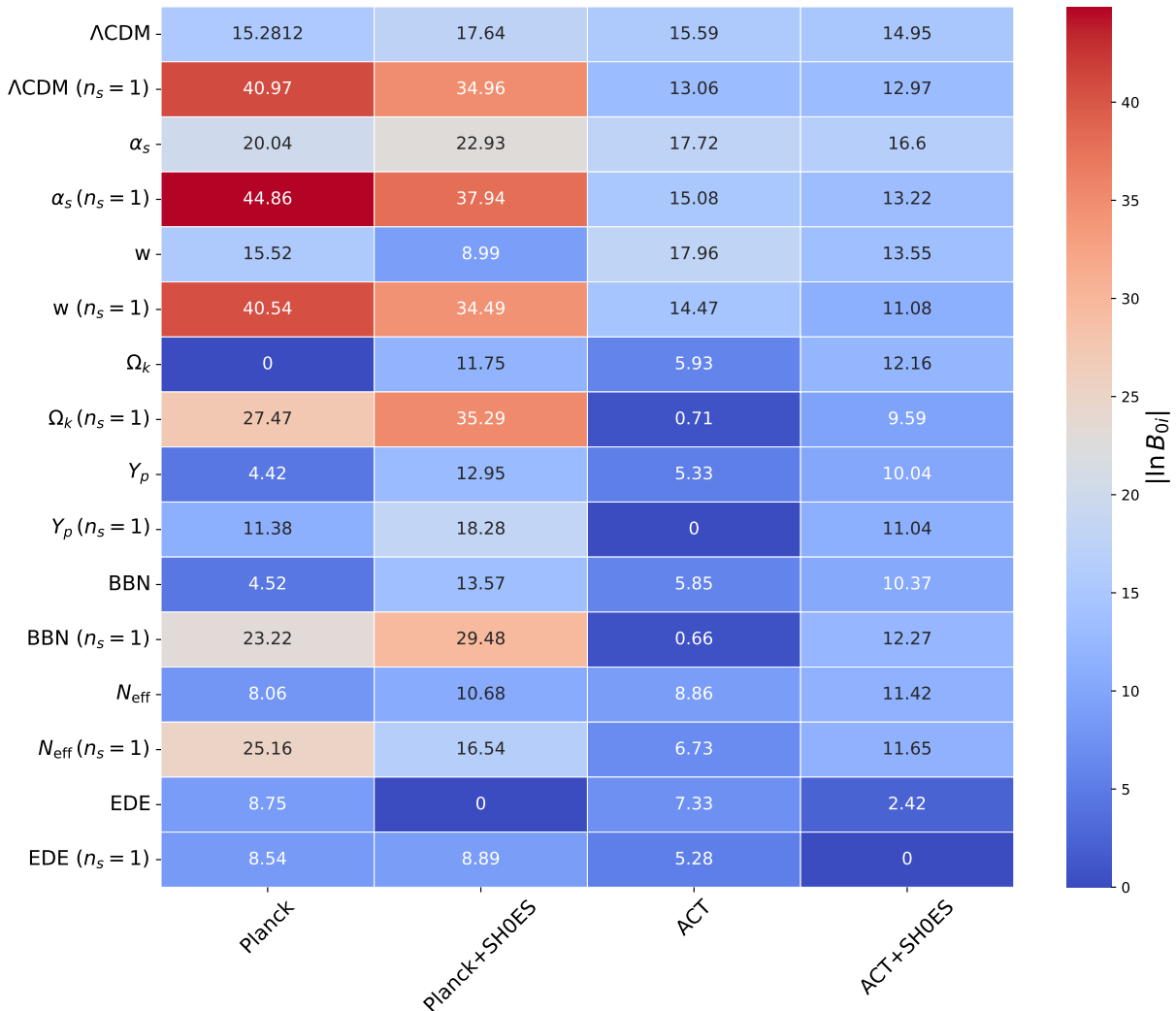


Figure 5: Bayesian factor B_{01} as presented in Eq. (12). To compute the preference for a model \mathcal{M}_1 with respect to \mathcal{M}_0 , we compare it with the modified Jeffreys' scale (see Sec. III A). In this case, \mathcal{M}_0 is the model with the lowest Bayesian evidence (see Eq. (10)) and is assigned a Bayesian factor of 0. Each column represents the Bayesian factor for a specific dataset combination.

Fixing n_s does not alleviate the tension for Planck, as Q_{DMAP} diminishes less effectively than in the standard scenario; for ACT, it remains near the ΛCDM value:

$$Q_{\text{DMAP}} = 5.05 \xrightarrow{n_s=1} 3.58 \quad (\text{Planck})$$

$$Q_{\text{DMAP}} = 3.88 \xrightarrow{n_s=1} 3.69 \quad (\text{ACT}).$$

Imposing a BBN prior likewise does not substantially shift Q_{DMAP} , except that it restores a more standard behavior for Planck with $n_s = 1$.

$\Lambda\text{CDM} + Y_p$ generally tracks ΛCDM in terms of the ΔAIC results reported in Tab. V. Introducing a BBN prior, however, yields strong evidence for all four data combinations if n_s is free. Instead, if we fix n_s , only ACT data favor this extension, with positive values such as $\Delta\text{AIC} = 4.95$ (with SH0ES) and $\Delta\text{AIC} = 7.62$ (without

SH0ES).

At 68% CL, Planck constrains $Y_p = 0.240 \pm 0.013$, which increases to $Y_p = 0.2929 \pm 0.0074$ when $n_s = 1$; notably, this is higher than typical BBN predictions. The increase is less pronounced with ACT, where $Y_p = 0.205 \pm 0.031$ rises to $Y_p = 0.226 \pm 0.017$ if $n_s = 1$. The constraints on the Helium abundance are sensitive to the inclusion of SH0ES when n_s is free, as the Helium fraction shifts to $Y_p = 0.258 \pm 0.013$ for Planck and $Y_p = 0.242 \pm 0.029$ for ACT. On the contrary, if $n_s = 1$, the constraints remain approximately the same.

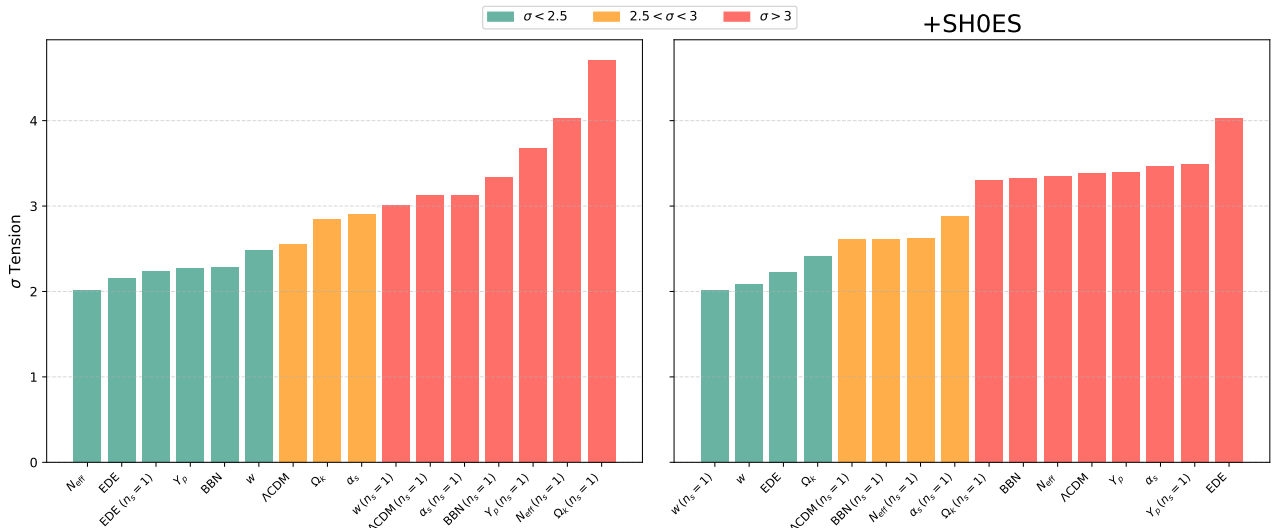


Figure 6: Here, we report the tension level $\sigma(p)$ as computed in Eq. (18), illustrating how the agreement between Planck and ACT varies according to the underlying cosmology.

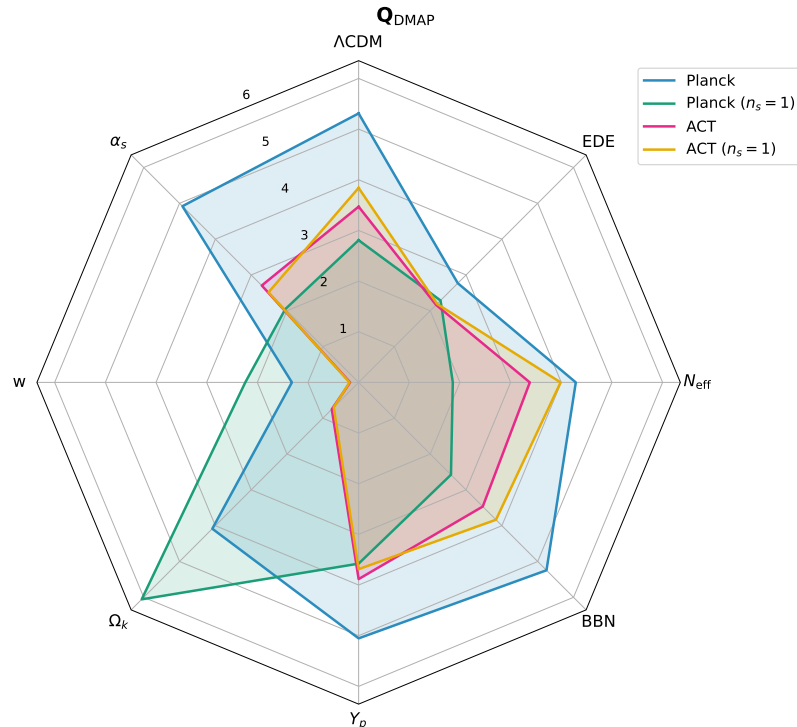


Figure 7: With this plot, we represent the Q_{DMAP} values for the different models. Q_{DMAP} has been computed following Eq. (19) and assigning $\chi^2_{\text{SH0ES}} \equiv 0$, as explained in Sec. IV.

6. $\Lambda\text{CDM} + N_{\text{eff}}$

Allowing the effective number of relativistic species N_{eff} to vary provides the best framework for studying the

disagreement between Planck and ACT without SH0ES, achieving a tension probability of $p = 4.4\%$, the highest among the models examined (see Tab. VI). Once SH0ES data are included, however, this probability falls to $p = 0.08\%$. Enforcing $n_s = 1$ drives the tension above

Model	χ^2	logS	p[%]	σ
Without SH0ES				
n_s free				
Λ CDM	16.67	-5.33	1.06	2.56
Λ CDM+ α_s	21.02	-7.01	0.37	2.90
w CDM	17.75	-5.38	1.31	2.48
Λ CDM+ Ω_k	20.55	-6.77	0.45	2.84
Λ CDM+ Y_p	16.24	-4.62	2.30	2.27
Λ CDM+BBN	16.34	-4.67	2.22	2.29
Λ CDM+ N_{eff}	14.42	-3.71	4.42	2.01
EDE	18.41	-4.71	3.07	2.16
n_s fixed				
Λ CDM	19.19	-7.09	0.18	3.13
Λ CDM+ α_s	21.11	-7.56	0.17	3.13
w CDM	20.10	-7.05	0.27	3.00
Λ CDM+ Ω_k	36.25	-15.12	0.0002	4.71
Λ CDM+ Y_p	25.88	-9.94	0.023	3.68
Λ CDM+BBN	22.88	-8.44	0.084	3.34
Λ CDM+ N_{eff}	29.17	-11.58	0.0061	4.03
EDE	17.48	-4.74	2.54	2.23
With SH0ES				
n_s free				
Λ CDM	23.25	-8.63	0.072	3.38
Λ CDM+ α_s	25.89	-9.44	0.053	3.47
w CDM	14.90	-3.95	3.72	2.08
Λ CDM+ Ω_k	17.22	-5.11	1.60	2.41
Λ CDM+ Y_p	25.22	-9.12	0.069	3.39
Λ CDM+BBN	24.64	-8.82	0.088	3.33
Λ CDM+ N_{eff}	24.87	-8.94	0.080	3.35
EDE	18.94	-4.97	2.57	2.23
n_s fixed				
Λ CDM	15.30	-5.15	0.92	2.61
Λ CDM+ α_s	19.13	-6.56	0.40	2.88
w CDM	14.42	-3.71	4.42	2.01
Λ CDM+ Ω_k	22.59	-8.29	0.095	3.31
Λ CDM+ Y_p	24.20	-9.10	0.048	3.49
Λ CDM+BBN	17.09	-5.54	0.90	2.61
Λ CDM+ N_{eff}	17.17	-5.58	0.87	2.62
EDE	33.22	-12.61	0.0056	4.03

Table VI: The compatibility between Planck and ACT has been computed using the suspiciousness $\log S$ defined in Eq. (15). To better estimate the tension, we also report the χ^2 value as defined in Eq. (16), the probability p (see Eq. (17)), and the tension level $\sigma(p)$ (as in Eq. (18)).

Model	Planck	ACT
n_s free		
Λ CDM	5.31	3.47
Λ CDM+ α_s	4.92	2.70
w CDM	1.32	0.17
Λ CDM+ Ω_k	4.09	0.75
Λ CDM+ Y_p	5.05	3.88
Λ CDM+BBN	5.24	3.47
Λ CDM+ N_{eff}	4.29	3.38
EDE	2.77	2.16
n_s fixed		
Λ CDM	2.81	3.84
Λ CDM+ α_s	2.05	2.52
w CDM	2.24	0.18
Λ CDM+ Ω_k	6.06	0.69
Λ CDM+ Y_p	3.58	3.69
Λ CDM+BBN	2.58	3.83
Λ CDM+ N_{eff}	1.86	3.99
EDE	2.29	2.19

Table VII: Here, we report the Q_{DMAP} values for the different models, with and without fixing an HZ spectrum. Q_{DMAP} measures the compatibility of explaining the data by combining two datasets instead of considering them independently. In this case, the comparison has been performed between Planck/ACT and SH0ES, thus quantifying the Hubble tension.

Q_{DMAP} has been computed using Eq. (19) and assigning $\chi^2_{\text{SH0ES}} \equiv 0$, as explained in Sec. IV.

4σ , both with and without SH0ES.

For Planck and ACT individually, adding N_{eff} does not dramatically affect the Hubble tension unless n_s is fixed. Under an HZ spectrum, Planck exhibits a large decrease, whereas for ACT it remains almost unchanged:

$$Q_{\text{DMAP}} = 4.29 \xrightarrow{n_s=1} 1.86 \quad (\text{Planck})$$

$$Q_{\text{DMAP}} = 3.38 \xrightarrow{n_s=1} 3.99 \quad (\text{ACT})$$

Examining the ΔAIC values in Tab. V, this extension of the standard model is generally not favored over Λ CDM; most cases show at least a *positive* preference for Λ CDM, except for ACT+SH0ES with n_s free, where the evidence is only *weak*, and Planck+SH0ES (n_s free), which notably shows *weak* evidence in favor of this alternative model, with $\Delta\text{AIC}=3.59$.

In the HZ spectrum scenario, Planck requires significantly more relativistic degrees of freedom, with $N_{\text{eff}} = 3.71 \pm 0.11$ at 68% CL, and this remains stable after adding SH0ES. Conversely, ACT data indicate only a small deviation from the standard expectation value [7],

which actually increases when $n_s = 1$, yielding $N_{\text{eff}} = 2.81 \pm 0.021$ at 68% CL.

7. EDE

Early Dark Energy proves highly effective at addressing the Planck and ACT tension, consistently yielding tension levels below 2.3σ . EDE with $n_s = 1$ achieves the best tension probability among all the extensions considered, while EDE with free n_s is the second-best. Including SH0ES retains a relatively high suspiciousness, but combining SH0ES with an HZ spectrum dramatically reverses the conclusions, with tensions beyond 4σ :

$$\log S = -4.71 \xrightarrow{n_s=1} -4.74 \quad (\text{without SH0ES})$$

$$\log S = -4.97 \xrightarrow{n_s=1} -12.61 \quad (\text{with SH0ES})$$

EDE is also the best model for alleviating the Hubble tension with Planck alone: $Q_{\text{DMAP}} = 2.77$. It remains almost stable when we change the assumption on n_s , as it ranges from 2.77 to 2.29 when we fix it. For ACT, Q_{DMAP} shows an even smaller excursion, with $Q_{\text{DMAP}} = 2.16$ increasing slightly to $Q_{\text{DMAP}} = 2.19$.

Turning to the ΔAIC values in Tab. V, the best performance of this model, as expected, is when SH0ES is combined with Planck. In fact, we obtain very strong evidence whether n_s is a free parameter or fixed, with $\Delta\text{AIC} = 16.05$ and $\Delta\text{AIC} = 13.93$, respectively. Planck-only data do not favor EDE over ΛCDM , while ACT-only indicates *weak* support when $n_s = 1$ and slightly disfavors it when n_s is free. In contrast, for ACT+SH0ES, there is strong evidence for EDE in both cases.

The bound obtained with Planck alone for the fraction of EDE shifts to nonzero values when SH0ES is included. The preference for a nonzero EDE component increases under the HZ scenario, with $f_{\text{EDE}} = 0.135 \pm 0.020$ at 68% CL for Planck, and a similar value for Planck+SH0ES. On the other hand, ACT displays the opposite behavior: for ACT+SH0ES, the fraction changes from $f_{\text{EDE}} = 0.123 \pm 0.031$ (n_s free) to $f_{\text{EDE}} = 0.106 \pm 0.027$ ($n_s = 1$), both at 68% CL, with a similar trend in ACT-only analyses.

VI. CONCLUSIONS

In this work, we have explored a variety of beyond- ΛCDM extensions to reconcile Planck and ACT datasets. We include modified geometry ($\Omega_k \neq 0$), running of the spectral index ($\alpha_s \neq 0$), a general dark energy equation of state ($w \neq -1$), extra relativistic species ($N_{\text{eff}} \neq 3.044$), a free primordial helium fraction (Y_p), also combined with a prior from BBN measurements, and early dark energy. For each case, we also impose a Harrison-Zel'dovich spectrum ($n_s = 1$) to test its impact on the overall parameter constraints, dataset consistency, and the Hubble tension.

To quantify the model's performance, we employ multiple statistical tools. We test the overall preference of a fixed dataset combination for an alternative model using the ΔAIC and Bayes factor. Our results align with previous conclusions presented in the literature, indicating that $\Lambda\text{CDM} + \Omega_k$ and EDE are the preferred models for Planck and Planck+SH0ES, respectively. On the other hand, ACT favors Y_p as a free parameter, while ACT+SH0ES prefers EDE, both combined with an HZ spectrum. The ΔAIC results yield similar, though not identical, preferences, as ACT favors $\Lambda\text{CDM} + \text{BBN}$, while ACT+SH0ES selects $\Lambda\text{CDM} + \Omega_k$. This highlights the simplistic penalization of extra parameters in the Akaike criterion, which, while useful for broad comparisons due to its widespread use, does not fully capture the complexity of parameter constraints in cosmological models.

The spectral index is more sensitive to the underlying cosmology, with Planck and ACT agreeing at the 1σ level when considering extensions that include the running of the spectral index, the helium fraction, the effective number of relativistic species, and early dark energy. However, when combined with SH0ES, these tensions increase. Conversely, $\Omega_b h^2$ is not significantly affected by the inclusion of SH0ES, while imposing a Harrison-Zel'dovich spectrum increases the discrepancy between values.

In terms of the tension between Planck and ACT, we note that the lowest tension levels occur for $\Lambda\text{CDM} + N_{\text{eff}}$, EDE, and EDE+ $n_s = 1$ when SH0ES is not included, and for $w\text{CDM} + n_s = 1$, $w\text{CDM}$, and EDE when SH0ES is included. However, the tension probability never exceeds $p = 4.4\%$.

Concerning the Hubble tension, the Q_{DMAP} values tend to diminish when the spectral index is fixed to unity in the Planck dataset, with all models presenting a lower value than $Q_{\text{DMAP}}^{\Lambda\text{CDM}} = 5.31$, except for the free-curvature case. ACT does not exhibit major differences with or without an HZ spectrum.

Overall, we find that no single extension entirely resolves the tensions among Planck, ACT, and SH0ES. From a physical standpoint, these findings underscore that small modifications to the standard model may not suffice to explain the issues observed in cosmological data. Even where statistical evidence marginally favors certain scenarios, significant residual discrepancies remain, raising the question of whether deeper extensions are needed. It is also possible that small systematic effects in CMB data or local H_0 determinations are magnified by the precision of modern measurements, highlighting the importance of improved calibration strategies and next-generation surveys.

While CMB measurements are often treated as the cornerstone of precision cosmology, the assumption that their systematics are fully under control may be overly optimistic. Planck, ACT, and SPT each employ different experimental designs, data processing pipelines, and foreground treatments, yet they do not always yield con-

sistent parameter constraints. The Planck-ACT tension, in particular, suggests that residual systematics may still be present, despite extensive efforts to account for them. Given that these datasets play a central role in defining the standard model of cosmology, it is crucial to adopt a more critical approach toward their uncertainties. Moving forward, independent analyses, cross-experiment consistency tests, and novel observational strategies will be essential in determining whether these tensions point to new physics or instead reflect limitations in our current understanding of the CMB.

As this work was being finalized, the new release of ACT-DR6 was announced. This upcoming dataset will provide a new opportunity to reassess the Planck-ACT inconsistency and test whether the tension persists. Whether this discrepancy remains or is alleviated with improved data will be of great interest to the commu-

nity.

ACKNOWLEDGMENTS

We thank WG for the interesting and useful discussions and for his contribution in developing the Cobaya wrapper for the MCEvidence and the Suspiciousness analysis. MF is funded by the PRIN (Progetti di ricerca di Rilevante Interesse Nazionale) number 2022WJ9J33. EDV is supported by a Royal Society Dorothy Hodgkin Research Fellowship. This article is based upon work from the COST Action CA21136 “Addressing observational tensions in cosmology with systematics and fundamental physics” (CosmoVerse), supported by COST (European Cooperation in Science and Technology). We acknowledge IT Services at The University of Sheffield for the provision of services for High Performance Computing.

-
- [1] D. J. Fixsen, E. S. Cheng, D. A. Cottingham, R. E. Eplee, Jr., R. B. Isaacman, J. C. Mather, S. S. Meyer, P. D. Noerdlinger, R. A. Shafer, R. Weiss, E. L. Wright, C. L. Bennett, N. W. Boggess, T. Kelsall, S. H. Moseley, R. F. Silverberg, G. F. Smoot, and D. T. Wilkinson, *Astrophys. J.* **420**, 445 (1994).
 - [2] C. L. Bennett, A. Banday, K. M. Gorski, G. Hinshaw, P. Jackson, P. Keegstra, A. Kogut, G. F. Smoot, D. T. Wilkinson, and E. L. Wright, *Astrophys. J. Lett.* **464**, L1 (1996), arXiv:astro-ph/9601067.
 - [3] G. Hinshaw, D. Larson, E. Komatsu, D. N. Spergel, C. L. Bennett, J. Dunkley, M. R. Nolta, M. Halpern, R. S. Hill, N. Odegard, L. Page, K. M. Smith, J. L. Weiland, B. Gold, N. Jarosik, A. Kogut, M. Limon, S. S. Meyer, G. S. Tucker, E. Wollack, and E. L. Wright, *Astrophys. J. Suppl.* **208**, 19 (2013), arXiv:1212.5226 [astro-ph.CO].
 - [4] C. L. Bennett, D. Larson, J. L. Weiland, N. Jarosik, G. Hinshaw, N. Odegard, K. M. Smith, R. S. Hill, B. Gold, M. Halpern, E. Komatsu, M. R. Nolta, L. Page, D. N. Spergel, E. Wollack, J. Dunkley, A. Kogut, M. Limon, S. S. Meyer, G. S. Tucker, and E. L. Wright, *Astrophys. J. Suppl.* **208**, 20 (2013), arXiv:1212.5225 [astro-ph.CO].
 - [5] N. Aghanim *et al.* (Planck), *Astron. Astrophys.* **641**, A6 (2020), [Erratum: *Astron. Astrophys.* 652, C4 (2021)], arXiv:1807.06209 [astro-ph.CO].
 - [6] S. K. Choi *et al.* (ACT), *JCAP* **12**, 045 (2020), arXiv:2007.07289 [astro-ph.CO].
 - [7] S. Aiola *et al.* (ACT), *JCAP* **12**, 047 (2020), arXiv:2007.07288 [astro-ph.CO].
 - [8] B. A. Benson *et al.* (SPT-3G), *Proc. SPIE Int. Soc. Opt. Eng.* **9153**, 91531P (2014), arXiv:1407.2973 [astro-ph.IM].
 - [9] D. Dutcher *et al.* (SPT-3G), *Phys. Rev. D* **104**, 022003 (2021), arXiv:2101.01684 [astro-ph.CO].
 - [10] L. Balkenhol *et al.* (SPT-3G), *Phys. Rev. D* **104**, 083509 (2021), arXiv:2103.13618 [astro-ph.CO].
 - [11] A. H. Guth, *Phys. Rev. D* **23**, 347 (1981).
 - [12] E. Abdalla *et al.*, *JHEAp* **34**, 49 (2022), arXiv:2203.06142 [astro-ph.CO].
 - [13] E. Di Valentino, *Universe* **8**, 399 (2022).
 - [14] L. Perivolaropoulos and F. Skara, *New Astronomy Rev.* **95**, 101659 (2022), arXiv:2105.05208 [astro-ph.CO].
 - [15] A. G. Riess, *Nature Rev. Phys.* **2**, 10 (2019), arXiv:2001.03624 [astro-ph.CO].
 - [16] E. Di Valentino, *Mon. Not. Roy. Astron. Soc.* **502**, 2065 (2021), arXiv:2011.00246 [astro-ph.CO].
 - [17] S. Vagnozzi, *Universe* **9**, 393 (2023), arXiv:2308.16628 [astro-ph.CO].
 - [18] L. Verde, T. Treu, and A. G. Riess, *Nature Astron.* **3**, 891 (2019), arXiv:1907.10625 [astro-ph.CO].
 - [19] E. Di Valentino *et al.*, *Astropart. Phys.* **131**, 102605 (2021), arXiv:2008.11284 [astro-ph.CO].
 - [20] E. Di Valentino, O. Mena, S. Pan, L. Visinelli, W. Yang, A. Melchiorri, D. F. Mota, A. G. Riess, and J. Silk, *Class. Quant. Grav.* **38**, 153001 (2021), arXiv:2103.01183 [astro-ph.CO].
 - [21] N. Schöneberg, G. Franco Abellán, A. Pérez Sánchez, S. J. Witte, V. Poulin, and J. Lesgourgues, *Phys. Rept.* **984**, 1 (2022), arXiv:2107.10291 [astro-ph.CO].
 - [22] P. Shah, P. Lemos, and O. Lahav, *Astron. Astrophys. Rev.* **29**, 9 (2021), arXiv:2109.01161 [astro-ph.CO].
 - [23] M. Kamionkowski and A. G. Riess, *Ann. Rev. Nucl. Part. Sci.* **73**, 153 (2023), arXiv:2211.04492 [astro-ph.CO].
 - [24] W. Giarè, “CMB Anomalies and the Hubble Tension,” (2023), arXiv:2305.16919 [astro-ph.CO].
 - [25] J.-P. Hu and F.-Y. Wang, *Universe* **9**, 94 (2023), arXiv:2302.05709 [astro-ph.CO].
 - [26] L. Verde, N. Schöneberg, and H. Gil-Marín, “A tale of many H_0 ,” (2023), arXiv:2311.13305 [astro-ph.CO].
 - [27] E. Di Valentino and D. Brout, eds., *The Hubble Constant Tension*, Springer Series in Astrophysics and Cosmology (Springer, 2024).
 - [28] L. Perivolaropoulos, “Hubble Tension or Distance Ladder Crisis?” (2024), arXiv:2408.11031 [astro-ph.CO].
 - [29] W. L. Freedman, B. F. Madore, T. Hoyt, I. S. Jang, R. Beaton, M. G. Lee, A. Monson, J. Neeley, and

- J. Rich, *Astrophys. J.* **891**, 57 (2020), arXiv:2002.01550 [astro-ph.GA].
- [30] S. Birrer *et al.*, *Astron. Astrophys.* **643**, A165 (2020), arXiv:2007.02941 [astro-ph.CO].
- [31] Q. Wu, G.-Q. Zhang, and F.-Y. Wang, *Mon. Not. Roy. Astron. Soc.* **515**, L1 (2022), [Erratum: Mon.Not.Roy.Astron.Soc. 531, L8 (2024)], arXiv:2108.00581 [astro-ph.CO].
- [32] R. I. Anderson, N. W. Koblischke, and L. Eyer, *Astrophys. J. Lett.* **963**, L43 (2024), arXiv:2303.04790 [astro-ph.CO].
- [33] D. Scolnic, A. G. Riess, J. Wu, S. Li, G. S. Anand, R. Beaton, S. Casertano, R. I. Anderson, S. Dhawan, and X. Ke, *Astrophys. J. Lett.* **954**, L31 (2023), arXiv:2304.06693 [astro-ph.CO].
- [34] D. O. Jones *et al.*, *Astrophys. J.* **933**, 172 (2022), arXiv:2201.07801 [astro-ph.CO].
- [35] G. S. Anand, R. B. Tully, L. Rizzi, A. G. Riess, and W. Yuan, *Astrophys. J.* **932**, 15 (2022), arXiv:2108.00007 [astro-ph.CO].
- [36] W. L. Freedman, *Astrophys. J.* **919**, 16 (2021), arXiv:2106.15656 [astro-ph.CO].
- [37] S. A. Uddin *et al.*, *Astrophys. J.* **970**, 72 (2024), arXiv:2308.01875 [astro-ph.CO].
- [38] C. D. Huang *et al.*, *Astrophys. J.* **963**, 83 (2024), arXiv:2312.08423 [astro-ph.CO].
- [39] S. Li, A. G. Riess, S. Casertano, G. S. Anand, D. M. Scolnic, W. Yuan, L. Breuval, and C. D. Huang, *Astrophys. J.* **966**, 20 (2024), arXiv:2401.04777 [astro-ph.CO].
- [40] D. W. Pesce *et al.*, *Astrophys. J. Lett.* **891**, L1 (2020), arXiv:2001.09213 [astro-ph.CO].
- [41] E. Kourkchi, R. B. Tully, G. S. Anand, H. M. Courtois, A. Dupuy, J. D. Neill, L. Rizzi, and M. Seibert, *Astrophys. J.* **896**, 3 (2020), arXiv:2004.14499 [astro-ph.GA].
- [42] J. Schombert, S. McGaugh, and F. Lelli, *Astron. J.* **160**, 71 (2020), arXiv:2006.08615 [astro-ph.CO].
- [43] J. P. Blakeslee, J. B. Jensen, C.-P. Ma, P. A. Milne, and J. E. Greene, *Astrophys. J.* **911**, 65 (2021), arXiv:2101.02221 [astro-ph.CO].
- [44] T. de Jaeger, L. Galbany, A. G. Riess, B. E. Stahl, B. J. Shappee, A. V. Filippenko, and W. Zheng, *Mon. Not. Roy. Astron. Soc.* **514**, 4620 (2022), arXiv:2203.08974 [astro-ph.CO].
- [45] Y. S. Murakami, A. G. Riess, B. E. Stahl, W. D. Kenworthy, D.-M. A. Pluck, A. Macorettta, D. Brout, D. O. Jones, D. M. Scolnic, and A. V. Filippenko, *JCAP* **11**, 046 (2023), arXiv:2306.00070 [astro-ph.CO].
- [46] L. Breuval, A. G. Riess, S. Casertano, W. Yuan, L. M. Macri, M. Romaniello, Y. S. Murakami, D. Scolnic, G. S. Anand, and I. Soszyński, *Astrophys. J.* **973**, 30 (2024), arXiv:2404.08038 [astro-ph.CO].
- [47] W. L. Freedman, B. F. Madore, I. S. Jang, T. J. Hoyt, A. J. Lee, and K. A. Owens, “Status Report on the Chicago-Carnegie Hubble Program (CCHP): Three Independent Astrophysical Determinations of the Hubble Constant Using the James Webb Space Telescope,” (2024), arXiv:2408.06153 [astro-ph.CO].
- [48] A. G. Riess *et al.*, “JWST Validates HST Distance Measurements: Selection of Supernova Subsample Explains Differences in JWST Estimates of Local H_0 ,” (2024), arXiv:2408.11770 [astro-ph.CO].
- [49] C. Vogl *et al.*, “No rungs attached: A distance-ladder free determination of the Hubble constant through type II supernova spectral modelling,” (2024), arXiv:2411.04968 [astro-ph.CO].
- [50] D. H. Gao, Q. Wu, J. P. Hu, S. X. Yi, X. Zhou, and F. Y. Wang, “Measuring Hubble constant using localized and unlocalized fast radio bursts,” (2024), arXiv:2410.03994 [astro-ph.CO].
- [51] D. Scolnic *et al.*, “The Hubble Tension in our own Backyard: DESI and the Nearness of the Coma Cluster,” (2024), arXiv:2409.14546 [astro-ph.CO].
- [52] K. Said *et al.*, “DESI Peculiar Velocity Survey – Fundamental Plane,” (2024), arXiv:2408.13842 [astro-ph.CO].
- [53] P. Boubel, M. Colless, K. Said, and L. Staveley-Smith, *Mon. Not. Roy. Astron. Soc.* **533**, 1550 (2024), arXiv:2408.03660 [astro-ph.CO].
- [54] P. A. R. Ade *et al.* (Planck), *Astron. Astrophys.* **571**, A16 (2014), arXiv:1303.5076 [astro-ph.CO].
- [55] E. Di Valentino, S. Galli, M. Lattanzi, A. Melchiorri, P. Natoli, L. Pagano, and N. Said, *Phys. Rev. D* **88**, 023501 (2013), arXiv:1301.7343 [astro-ph.CO].
- [56] P. A. R. Ade *et al.* (Planck), *Astron. Astrophys.* **594**, A13 (2016), arXiv:1502.01589 [astro-ph.CO].
- [57] G. E. Addison, Y. Huang, D. J. Watts, C. L. Bennett, M. Halpern, G. Hinshaw, and J. L. Weiland, *Astrophys. J.* **818**, 132 (2016), arXiv:1511.00055 [astro-ph.CO].
- [58] N. Aghanim *et al.* (Planck), *Astron. Astrophys.* **607**, A95 (2017), arXiv:1608.02487 [astro-ph.CO].
- [59] F. Renzi, E. Di Valentino, and A. Melchiorri, *Phys. Rev. D* **97**, 123534 (2018), arXiv:1712.08758 [astro-ph.CO].
- [60] E. Di Valentino, E. V. Linder, and A. Melchiorri, *Phys. Rev. D* **97**, 043528 (2018), arXiv:1710.02153 [astro-ph.CO].
- [61] G. E. Addison, C. L. Bennett, M. Halpern, G. Hinshaw, and J. L. Weiland, *Astrophys. J.* **974**, 187 (2024), arXiv:2310.03127 [astro-ph.CO].
- [62] I. Ben-Dayan, U. Kumar, M. Shimon, and A. Verma, *JCAP* **02**, 069 (2025), arXiv:2409.15457 [astro-ph.CO].
- [63] E. Specogna, W. Giarè, and E. Di Valentino, “Planck-PR4 anisotropy spectra show (better) consistency with General Relativity,” (2024), arXiv:2411.03896 [astro-ph.CO].
- [64] E. Rosenberg, S. Gratton, and G. Efstathiou, *Mon. Not. Roy. Astron. Soc.* **517**, 4620 (2022), arXiv:2205.10869 [astro-ph.CO].
- [65] W. Handley, *Phys. Rev. D* **103**, L041301 (2021), arXiv:1908.09139 [astro-ph.CO].
- [66] E. Di Valentino *et al.*, *Astropart. Phys.* **131**, 102607 (2021), arXiv:2008.11286 [astro-ph.CO].
- [67] S. Vagnozzi, E. Di Valentino, S. Gariazzo, A. Melchiorri, O. Mena, and J. Silk, *Phys. Dark Univ.* **33**, 100851 (2021), arXiv:2010.02230 [astro-ph.CO].
- [68] Z. Shumaylov and W. Handley, *Phys. Rev. D* **105**, 123532 (2022), arXiv:2112.07547 [astro-ph.CO].
- [69] W. Yang, W. Giarè, S. Pan, E. Di Valentino, A. Melchiorri, and J. Silk, *Phys. Rev. D* **107**, 063509 (2023), arXiv:2210.09865 [astro-ph.CO].
- [70] A. Glanville, C. Howlett, and T. M. Davis, *Mon. Not. Roy. Astron. Soc.* **517**, 3087 (2022), arXiv:2205.05892 [astro-ph.CO].
- [71] E. Di Valentino, A. Melchiorri, and J. Silk, *Astrophys. J. Lett.* **908**, L9 (2021), arXiv:2003.04935 [astro-ph.CO].
- [72] S. Anselmi, M. F. Carney, J. T. Giblin, S. Kumar, J. B. Mertens, M. O’Dwyer, G. D. Starkman, and C. Tian, *JCAP* **02**, 049 (2023), arXiv:2207.06547 [astro-ph.CO].

- [73] W. Lin and M. Ishak, *JCAP* **05**, 009 (2021), arXiv:1909.10991 [astro-ph.CO].
- [74] W. Handley and P. Lemos, *Phys. Rev. D* **103**, 063529 (2021), arXiv:2007.08496 [astro-ph.CO].
- [75] E. Di Valentino, W. Giarè, A. Melchiorri, and J. Silk, *Mon. Not. Roy. Astron. Soc.* **520**, 210 (2023), arXiv:2209.14054 [astro-ph.CO].
- [76] A. La Posta, U. Natale, E. Calabrese, X. Garrido, and T. Louis, *Phys. Rev. D* **107**, 023510 (2023), arXiv:2204.01885 [astro-ph.CO].
- [77] R. Calderón, A. Shafieloo, D. K. Hazra, and W. Sohn, *JCAP* **08**, 059 (2023), arXiv:2302.14300 [astro-ph.CO].
- [78] J.-Q. Jiang and Y.-S. Piao, *Phys. Rev. D* **105**, 103514 (2022), arXiv:2202.13379 [astro-ph.CO].
- [79] E. Di Valentino, A. Melchiorri, Y. Fantaye, and A. Heavens, *Phys. Rev. D* **98**, 063508 (2018), arXiv:1808.09201 [astro-ph.CO].
- [80] G. Ye, J.-Q. Jiang, and Y.-S. Piao, *Phys. Rev. D* **106**, 103528 (2022), arXiv:2205.02478 [astro-ph.CO].
- [81] J.-Q. Jiang, G. Ye, and Y.-S. Piao, *Mon. Not. Roy. Astron. Soc.* **527**, L54 (2023), arXiv:2210.06125 [astro-ph.CO].
- [82] W. Giarè, S. Pan, E. Di Valentino, W. Yang, J. de Haro, and A. Melchiorri, *JCAP* **09**, 019 (2023), arXiv:2305.15378 [astro-ph.CO].
- [83] E. Di Valentino, W. Giarè, A. Melchiorri, and J. Silk, *Phys. Rev. D* **106**, 103506 (2022), arXiv:2209.12872 [astro-ph.CO].
- [84] M. Forconi, W. Giarè, E. Di Valentino, and A. Melchiorri, *Phys. Rev. D* **104**, 103528 (2021), arXiv:2110.01695 [astro-ph.CO].
- [85] E. Di Valentino and A. Melchiorri, *Astrophys. J. Lett.* **931**, L18 (2022), arXiv:2112.02993 [astro-ph.CO].
- [86] J. C. Hill *et al.*, *Phys. Rev. D* **105**, 123536 (2022), arXiv:2109.04451 [astro-ph.CO].
- [87] V. Poulin, T. L. Smith, and A. Bartlett, *Phys. Rev. D* **104**, 123550 (2021), arXiv:2109.06229 [astro-ph.CO].
- [88] W. Giarè, “Dynamical Dark Energy Beyond Planck? Constraints from multiple CMB probes, DESI BAO and Type-Ia Supernovae,” (2024), arXiv:2409.17074 [astro-ph.CO].
- [89] T. Charnock, R. A. Battye, and A. Moss, *Phys. Rev. D* **95**, 123535 (2017), arXiv:1703.05959 [astro-ph.CO].
- [90] W. Handley and P. Lemos, *Phys. Rev. D* **100**, 043504 (2019), arXiv:1902.04029 [astro-ph.CO].
- [91] D. K. Hazra, B. Beringue, J. Errard, A. Shafieloo, and G. F. Smoot, “Exploring the discrepancy between Planck PR3 and ACT DR4,” (2024), arXiv:2406.06296 [astro-ph.CO].
- [92] W. Giarè, F. Renzi, O. Mena, E. Di Valentino, and A. Melchiorri, *Mon. Not. Roy. Astron. Soc.* **521**, 2911 (2023), arXiv:2210.09018 [astro-ph.CO].
- [93] E. R. Harrison, *Phys. Rev. D* **1**, 2726 (1970).
- [94] Y. B. Zeldovich, *Mon. Not. Roy. Astron. Soc.* **160**, 1P (1972).
- [95] P. J. E. Peebles and J. T. Yu, *Astrophys. J.* **162**, 815 (1970).
- [96] A. Vallinotto, E. J. Copeland, E. W. Kolb, A. R. Liddle, and D. A. Steer, *Phys. Rev. D* **69**, 103519 (2004), arXiv:astro-ph/0311005.
- [97] M. Rinaldi and L. Vanzo, *Phys. Rev. D* **94**, 024009 (2016), arXiv:1512.07186 [gr-qc].
- [98] C. Cecchini, M. De Angelis, W. Giarè, M. Rinaldi, and S. Vagnozzi, *JCAP* **07**, 058 (2024), arXiv:2403.04316 [astro-ph.CO].
- [99] M. Rinaldi, C. Cecchini, A. Ghoshal, and D. Mukherjee, *J. Phys. Conf. Ser.* **2531**, 012012 (2023), arXiv:2303.16107 [gr-qc].
- [100] G. Ye, B. Hu, and Y.-S. Piao, *Phys. Rev. D* **104**, 063510 (2021), arXiv:2103.09729 [astro-ph.CO].
- [101] W. Giarè, *Phys. Rev. D* **109**, 123545 (2024), arXiv:2404.12779 [astro-ph.CO].
- [102] N. Aghanim *et al.* (Planck), *Astron. Astrophys.* **641**, A1 (2020), arXiv:1807.06205 [astro-ph.CO].
- [103] Y. Akrami *et al.* (Planck), *Astron. Astrophys.* **641**, A10 (2020), arXiv:1807.06211 [astro-ph.CO].
- [104] M. Benetti, L. L. Graef, and J. S. Alcaniz, *JCAP* **07**, 066 (2018), arXiv:1712.00677 [astro-ph.CO].
- [105] M. Benetti, L. L. Graef, and J. S. Alcaniz, *JCAP* **04**, 003 (2017), arXiv:1702.06509 [astro-ph.CO].
- [106] M. Benetti, M. Gerbino, W. H. Kinney, E. W. Kolb, M. Lattanzi, A. Melchiorri, L. Pagano, and A. Riotto, *JCAP* **10**, 030 (2013), arXiv:1303.4317 [astro-ph.CO].
- [107] S. Pandolfi, A. Cooray, E. Giusarma, E. W. Kolb, A. Melchiorri, O. Mena, and P. Serra, *Phys. Rev. D* **81**, 123509 (2010), arXiv:1003.4763 [astro-ph.CO].
- [108] A. Kosowsky and M. S. Turner, *Phys. Rev. D* **52**, R1739 (1995), arXiv:astro-ph/9504071.
- [109] J. E. Lidsey, A. R. Liddle, E. W. Kolb, E. J. Copeland, T. Barreiro, and M. Abney, *Rev. Mod. Phys.* **69**, 373 (1997), arXiv:astro-ph/9508078.
- [110] S. Kuroyanagi, T. Chiba, and N. Sugiyama, *Phys. Rev. D* **79**, 103501 (2009), arXiv:0804.3249 [astro-ph].
- [111] S. Kuroyanagi and T. Takahashi, *JCAP* **10**, 006 (2011), arXiv:1106.3437 [astro-ph.CO].
- [112] M. Zarei, *Class. Quant. Grav.* **33**, 115008 (2016), arXiv:1408.6467 [astro-ph.CO].
- [113] W. Giarè and A. Melchiorri, *Phys. Lett. B* **815**, 136137 (2021), arXiv:2003.04783 [astro-ph.CO].
- [114] W. Giarè and F. Renzi, *Phys. Rev. D* **102**, 083530 (2020), arXiv:2007.04256 [astro-ph.CO].
- [115] J. Li and Q.-G. Huang, *Eur. Phys. J. C* **78**, 980 (2018), arXiv:1806.01440 [astro-ph.CO].
- [116] W. Giarè, E. Di Valentino, and A. Melchiorri, *Phys. Rev. D* **99**, 123522 (2019).
- [117] J. Martin, C. Ringeval, and V. Vennin, *JCAP* **07**, 087 (2024), arXiv:2404.10647 [astro-ph.CO].
- [118] J. Martin, C. Ringeval, and V. Vennin, *EPL* **148**, 29002 (2024), arXiv:2404.15089 [astro-ph.CO].
- [119] J. Dunkley, R. Hlozek, J. Sievers, V. Acquaviva, P. A. R. Ade, P. Aguirre, M. Amiri, J. W. Appel, L. F. Barrientos, E. S. Battistelli, J. R. Bond, B. Brown, B. Burger, J. Chervenak, S. Das, M. J. Devlin, S. R. Dicker, W. Bertrand Doriese, R. Dünner, T. Essinger-Hileman, R. P. Fisher, J. W. Fowler, A. Hajian, M. Halpern, M. Hasselfield, C. Hernández-Monteagudo, G. C. Hilton, M. Hilton, A. D. Hincks, K. M. Huffenberger, D. H. Hughes, J. P. Hughes, L. Infante, K. D. Irwin, J. B. Juin, M. Kaul, J. Klein, A. Kosowsky, J. M. Lau, M. Limon, Y. T. Lin, R. H. Lupton, T. A. Marriage, D. Marsden, P. Mauskopf, F. Menanteau, K. Moodley, H. Moseley, C. B. Netterfield, M. D. Niemack, M. R. Nolta, L. A. Page, L. Parker, B. Partridge, B. Reid, N. Sehgal, B. Sherwin, D. N. Spergel, S. T. Staggs, D. S. Swetz, E. R. Switzer, R. Thornton, H. Trac, C. Tucker, R. Warne, E. Wollack, and Y. Zhao, *Astrophys. Journal* **739**, 52 (2011), arXiv:1009.0866 [astro-ph.CO].

- [120] R. Keisler, C. L. Reichardt, K. A. Aird, B. A. Benson, L. E. Bleem, J. E. Carlstrom, C. L. Chang, H. M. Cho, T. M. Crawford, A. T. Crites, T. de Haan, M. A. Dobbs, J. Dudley, E. M. George, N. W. Halverson, G. P. Holder, W. L. Holzapfel, S. Hoover, Z. Hou, J. D. Hrubes, M. Joy, L. Knox, A. T. Lee, E. M. Leitch, M. Lueker, D. Luong-Van, J. J. McMahon, J. Mehl, S. S. Meyer, M. Millea, J. J. Mohr, T. E. Montroy, T. Natoli, S. Padin, T. Plagge, C. Pryke, J. E. Ruhl, K. K. Schaffer, L. Shaw, E. Shirokoff, H. G. Spieler, Z. Staniszewski, A. A. Stark, K. Story, A. van Engelen, K. Vanderlinde, J. D. Vieira, R. Williamson, and O. Zahn, *Astrophys. Journal* **743**, 28 (2011), arXiv:1105.3182 [astro-ph.CO].
- [121] B. Bahr-Kalus, D. Parkinson, and R. Easther, *Mon. Not. Roy. Astron. Soc.* **520**, 2405 (2023), arXiv:2212.04115 [astro-ph.CO].
- [122] R. Easther, B. Bahr-Kalus, and D. Parkinson, *Phys. Rev. D* **106**, L061301 (2022), arXiv:2112.10922 [astro-ph.CO].
- [123] A. G. Riess *et al.* (Supernova Search Team), *Astron. J.* **116**, 1009 (1998), arXiv:astro-ph/9805201.
- [124] S. Perlmutter *et al.* (Supernova Cosmology Project), *Astrophys. J.* **517**, 565 (1999), arXiv:astro-ph/9812133.
- [125] B. D. Sherwin, J. Dunkley, S. Das, J. W. Appel, J. R. Bond, C. S. Carvalho, M. J. Devlin, R. Dünner, T. Essinger-Hileman, J. W. Fowler, A. Hajian, M. Halpern, M. Hasselfield, A. D. Hincks, R. Hlozek, J. P. Hughes, K. D. Irwin, J. Klein, A. Kosowsky, T. A. Marriage, D. Marsden, K. Moodley, F. Menanteau, M. D. Niemack, M. R. Nolta, L. A. Page, L. Parker, E. D. Reese, B. L. Schmitt, N. Sehgal, J. Sievers, D. N. Spergel, S. T. Staggs, D. S. Swetz, E. R. Switzer, R. Thornton, K. Visnjic, and E. Wollack, *Physical Review Letters* **107**, 021302 (2011), arXiv:1105.0419 [astro-ph.CO].
- [126] M. Moresco, L. Pozzetti, A. Cimatti, R. Jimenez, C. Maraston, L. Verde, D. Thomas, A. Citro, R. Tojeiro, and D. Wilkinson, *JCAP* **05**, 014 (2016), arXiv:1601.01701 [astro-ph.CO].
- [127] B. S. Haridasu, V. V. Luković, R. D’Agostino, and N. Vittorio, *Astron. Astrophys.* **600**, L1 (2017), arXiv:1702.08244 [astro-ph.CO].
- [128] R. R. Caldwell, M. Kamionkowski, and N. N. Weinberg, *Phys. Rev. Lett.* **91**, 071301 (2003), arXiv:astro-ph/0302506.
- [129] S. Nojiri, S. D. Odintsov, and S. Tsujikawa, *Phys. Rev. D* **71**, 063004 (2005), arXiv:hep-th/0501025.
- [130] P. H. Frampton, K. J. Ludwick, and R. J. Scherrer, *Phys. Rev. D* **84**, 063003 (2011), arXiv:1106.4996 [astro-ph.CO].
- [131] A. V. Astashenok, S. Nojiri, S. D. Odintsov, and A. V. Yurov, *Phys. Lett. B* **709**, 396 (2012), arXiv:1201.4056 [gr-qc].
- [132] S. D. Odintsov and V. K. Oikonomou, *Phys. Rev. D* **92**, 024016 (2015), arXiv:1504.06866 [gr-qc].
- [133] S. D. Odintsov and V. K. Oikonomou, *EPL* **126**, 20002 (2019), arXiv:1810.03575 [gr-qc].
- [134] C. Wetterich, *Nucl. Phys. B* **302**, 668 (1988), arXiv:1711.03844 [hep-th].
- [135] B. Ratra and P. J. E. Peebles, *Phys. Rev. D* **37**, 3406 (1988).
- [136] C. Wetterich, *Astron. Astrophys.* **301**, 321 (1995), arXiv:hep-th/9408025.
- [137] R. R. Caldwell, R. Dave, and P. J. Steinhardt, *Phys. Rev. Lett.* **80**, 1582 (1998), arXiv:astro-ph/9708069.
- [138] V. Sahni, *Class. Quant. Grav.* **19**, 3435 (2002), arXiv:astro-ph/0202076.
- [139] M. Moresco, R. Jimenez, L. Verde, A. Cimatti, L. Pozzetti, C. Maraston, and D. Thomas, *JCAP* **12**, 039 (2016), arXiv:1604.00183 [astro-ph.CO].
- [140] S. Alam *et al.* (eBOSS), *Phys. Rev. D* **103**, 083533 (2021), arXiv:2007.08991 [astro-ph.CO].
- [141] G. D’Amico, L. Senatore, P. Zhang, and H. Zheng, *JCAP* **05**, 072 (2021), arXiv:2006.12420 [astro-ph.CO].
- [142] C. Grillo, P. Rosati, S. H. Suyu, G. B. Caminha, A. Mercurio, and A. Halkola, *Astrophys. J.* **898**, 87 (2020), arXiv:2001.02232 [astro-ph.CO].
- [143] S. Cao, N. Khadka, and B. Ratra, *Mon. Not. Roy. Astron. Soc.* **510**, 2928 (2022), arXiv:2110.14840 [astro-ph.CO].
- [144] A. Chudaykin, K. Dolgikh, and M. M. Ivanov, *Phys. Rev. D* **103**, 023507 (2021), arXiv:2009.10106 [astro-ph.CO].
- [145] S. Vagnozzi, A. Loeb, and M. Moresco, *Astrophys. J.* **908**, 84 (2021), arXiv:2011.11645 [astro-ph.CO].
- [146] G. Bargiacchi, M. Benetti, S. Capozziello, E. Lusso, G. Risaliti, and M. Signorini, *Mon. Not. Roy. Astron. Soc.* **515**, 1795 (2022), arXiv:2111.02420 [astro-ph.CO].
- [147] M. Moresco *et al.*, *Living Rev. Rel.* **25**, 6 (2022), arXiv:2201.07241 [astro-ph.CO].
- [148] S. Brieden, H. Gil-Marín, and L. Verde, *JCAP* **04**, 023 (2023), arXiv:2212.04522 [astro-ph.CO].
- [149] P. Carrilho, C. Moretti, and A. Pourtsidou, *JCAP* **01**, 028 (2023), arXiv:2207.14784 [astro-ph.CO].
- [150] A. Semenaite, A. G. Sánchez, A. Pezzotta, J. Hou, A. Eggemeier, M. Crocce, C. Zhao, J. R. Brownstein, G. Rossi, and D. P. Schneider, *Mon. Not. Roy. Astron. Soc.* **521**, 5013 (2023), arXiv:2210.07304 [astro-ph.CO].
- [151] T. Tröster *et al.* (KiDS), *Astron. Astrophys.* **649**, A88 (2021), arXiv:2010.16416 [astro-ph.CO].
- [152] T. M. C. Abbott *et al.* (DES), *Phys. Rev. D* **107**, 083504 (2023), arXiv:2207.05766 [astro-ph.CO].
- [153] E. Di Valentino, S. Gariazzo, O. Mena, and S. Vagnozzi, *JCAP* **07**, 045 (2020), arXiv:2005.02062 [astro-ph.CO].
- [154] A. D. Linde, *Phys. Lett. B* **108**, 389 (1982).
- [155] A. D. Linde, *Phys. Lett. B* **129**, 177 (1983).
- [156] J. R. Bond, G. Efstathiou, and M. Tegmark, *Mon. Not. Roy. Astron. Soc.* **291**, L33 (1997), arXiv:astro-ph/9702100.
- [157] A. J. Ross, L. Samushia, C. Howlett, W. J. Percival, A. Burden, and M. Manera, *Mon. Not. Roy. Astron. Soc.* **449**, 835 (2015), arXiv:1409.3242 [astro-ph.CO].
- [158] S. Alam *et al.* (BOSS), *Mon. Not. Roy. Astron. Soc.* **470**, 2617 (2017), arXiv:1607.03155 [astro-ph.CO].
- [159] E. Di Valentino, A. Melchiorri, and J. Silk, *Nature Astron.* **4**, 196 (2019), arXiv:1911.02087 [astro-ph.CO].
- [160] G. Efstathiou and S. Gratton, “A Detailed Description of the CamSpec Likelihood Pipeline and a Re-analysis of the Planck High Frequency Maps,” (2019), arXiv:1910.00483 [astro-ph.CO].
- [161] G. Efstathiou and S. Gratton, *Mon. Not. Roy. Astron. Soc.* **496**, L91 (2020), arXiv:2002.06892 [astro-ph.CO].
- [162] M. Tristram *et al.*, *Astron. Astrophys.* **682**, A37 (2024), arXiv:2309.10034 [astro-ph.CO].
- [163] J. E. Gonzalez, M. Benetti, R. von Marttens, and J. Alcaniz, *JCAP* **11**, 060 (2021), arXiv:2104.13455 [astro-ph.CO].

- [164] A. Favale, A. Gómez-Valent, and M. Migliaccio, *Mon. Not. Roy. Astron. Soc.* **523**, 3406 (2023), arXiv:2301.09591 [astro-ph.CO].
- [165] J. Bel, J. Larena, R. Maartens, C. Marinoni, and L. Perenon, *JCAP* **09**, 076 (2022), arXiv:2206.03059 [astro-ph.CO].
- [166] L. Amendola, M. Marinucci, and M. Quartin, “Spatial curvature with the Alcock-Paczynski effect,” (2024), arXiv:2404.13124 [astro-ph.CO].
- [167] A. Peimbert, M. Peimbert, and V. Luridiana, *Rev. Mex. Astron. Astrofis.* **52**, 419 (2016), arXiv:1608.02062 [astro-ph.CO].
- [168] E. Aver, K. A. Olive, and E. D. Skillman, *JCAP* **07**, 011 (2015), arXiv:1503.08146 [astro-ph.CO].
- [169] P. D. Serpico, S. Esposito, F. Iocco, G. Mangano, G. Miele, and O. Pisanti, *JCAP* **12**, 010 (2004), arXiv:astro-ph/0408076.
- [170] A. D. Dolgov, S. H. Hansen, S. Pastor, S. T. Petcov, G. G. Raffelt, and D. V. Semikoz, *Nucl. Phys. B* **632**, 363 (2002), arXiv:hep-ph/0201287.
- [171] Y. Y. Y. Wong, *Phys. Rev. D* **66**, 025015 (2002), arXiv:hep-ph/0203180.
- [172] K. N. Abazajian, J. F. Beacom, and N. F. Bell, *Phys. Rev. D* **66**, 013008 (2002), arXiv:astro-ph/0203442.
- [173] G. Mangano, G. Miele, S. Pastor, and M. Peloso, *Phys. Lett. B* **534**, 8 (2002), arXiv:astro-ph/0111408.
- [174] J. J. Bennett, G. Buldgen, M. Drewes, and Y. Y. Y. Wong, *JCAP* **03**, 003 (2020), [Addendum: *JCAP* 03, A01 (2021)], arXiv:1911.04504 [hep-ph].
- [175] G. Mangano, G. Miele, S. Pastor, T. Pinto, O. Pisanti, and P. D. Serpico, *Nucl. Phys. B* **729**, 221 (2005), arXiv:hep-ph/0506164.
- [176] P. F. de Salas and S. Pastor, *JCAP* **07**, 051 (2016), arXiv:1606.06986 [hep-ph].
- [177] K. Akita and M. Yamaguchi, *JCAP* **08**, 012 (2020), arXiv:2005.07047 [hep-ph].
- [178] J. Froustey, C. Pitrou, and M. C. Volpe, *JCAP* **12**, 015 (2020), arXiv:2008.01074 [hep-ph].
- [179] J. J. Bennett, G. Buldgen, P. F. De Salas, M. Drewes, S. Gariazzo, S. Pastor, and Y. Y. Y. Wong, *JCAP* **04**, 073 (2021), arXiv:2012.02726 [hep-ph].
- [180] W. Giarè, M. Forconi, E. Di Valentino, and A. Melchiorri, *Mon. Not. Roy. Astron. Soc.* **520**, 2 (2023), arXiv:2210.14159 [astro-ph.CO].
- [181] P. F. de Salas, M. Lattanzi, G. Mangano, G. Miele, S. Pastor, and O. Pisanti, *Phys. Rev. D* **92**, 123534 (2015), arXiv:1511.00672 [astro-ph.CO].
- [182] A. G. Sanchez, *Phys. Rev. D* **102**, 123511 (2020), arXiv:2002.07829 [astro-ph.CO].
- [183] M. Forconi, A. Favale, and A. Gómez-Valent, “Illustrating the consequences of a misuse of σ_8 in cosmology,” (2025), arXiv:2501.11571 [astro-ph.CO].
- [184] S. Gariazzo, W. Giarè, O. Mena, and E. Di Valentino, *Phys. Rev. D* **111**, 023540 (2025), arXiv:2404.11182 [astro-ph.CO].
- [185] C. D. Kreisch *et al.*, *Phys. Rev. D* **109**, 043501 (2024), arXiv:2207.03164 [astro-ph.CO].
- [186] C. Wetterich, *Phys. Lett. B* **594**, 17 (2004), arXiv:astro-ph/0403289.
- [187] M. Doran and G. Robbers, *JCAP* **06**, 026 (2006), arXiv:astro-ph/0601544.
- [188] L. Hollenstein, D. Sapone, R. Crittenden, and B. M. Schaefer, *JCAP* **04**, 012 (2009), arXiv:0902.1494 [astro-ph.CO].
- [189] E. Calabrese, R. de Putter, D. Huterer, E. V. Linder, and A. Melchiorri, *Phys. Rev. D* **83**, 023011 (2011), arXiv:1010.5612 [astro-ph.CO].
- [190] E. Calabrese, D. Huterer, E. V. Linder, A. Melchiorri, and L. Pagano, *Phys. Rev. D* **83**, 123504 (2011), arXiv:1103.4132 [astro-ph.CO].
- [191] V. Pettorino, L. Amendola, and C. Wetterich, *Phys. Rev. D* **87**, 083009 (2013), arXiv:1301.5279 [astro-ph.CO].
- [192] M. Archidiacono, L. Lopez-Honorez, and O. Mena, *Phys. Rev. D* **90**, 123016 (2014), arXiv:1409.1802 [astro-ph.CO].
- [193] V. Poulin, T. L. Smith, and T. Karwal, *Phys. Dark Univ.* **42**, 101348 (2023), arXiv:2302.09032 [astro-ph.CO].
- [194] V. Poulin, T. L. Smith, D. Grin, T. Karwal, and M. Kamionkowski, *Phys. Rev. D* **98**, 083525 (2018), arXiv:1806.10608 [astro-ph.CO].
- [195] V. Poulin, K. K. Boddy, S. Bird, and M. Kamionkowski, *Phys. Rev. D* **97**, 123504 (2018), arXiv:1803.02474 [astro-ph.CO].
- [196] T. L. Smith, V. Poulin, and M. A. Amin, *Phys. Rev. D* **101**, 063523 (2020), arXiv:1908.06995 [astro-ph.CO].
- [197] F. Niedermann and M. S. Sloth, *Phys. Rev. D* **105**, 063509 (2022), arXiv:2112.00770 [hep-ph].
- [198] R. Murgia, G. F. Abellán, and V. Poulin, *Phys. Rev. D* **103**, 063502 (2021), arXiv:2009.10733 [astro-ph.CO].
- [199] G. Ye and Y.-S. Piao, *Phys. Rev. D* **101**, 083507 (2020), arXiv:2001.02451 [astro-ph.CO].
- [200] A. Klypin, V. Poulin, F. Prada, J. Primack, M. Kamionkowski, V. Avila-Reese, A. Rodriguez-Puebla, P. Behroozi, D. Hellinger, and T. L. Smith, *Mon. Not. Roy. Astron. Soc.* **504**, 769 (2021), arXiv:2006.14910 [astro-ph.CO].
- [201] J. C. Hill, E. McDonough, M. W. Toomey, and S. Alexander, *Phys. Rev. D* **102**, 043507 (2020), arXiv:2003.07355 [astro-ph.CO].
- [202] L. Herold, E. G. M. Ferreira, and E. Komatsu, *Astrophys. J. Lett.* **929**, L16 (2022), arXiv:2112.12140 [astro-ph.CO].
- [203] L. Herold and E. G. M. Ferreira, *Phys. Rev. D* **108**, 043513 (2023), arXiv:2210.16296 [astro-ph.CO].
- [204] A. Reeves, L. Herold, S. Vagnozzi, B. D. Sherwin, and E. G. M. Ferreira, *Mon. Not. Roy. Astron. Soc.* **520**, 3688 (2023), arXiv:2207.01501 [astro-ph.CO].
- [205] T. Simon, P. Zhang, V. Poulin, and T. L. Smith, *Phys. Rev. D* **107**, 063505 (2023), arXiv:2208.05930 [astro-ph.CO].
- [206] T. L. Smith, M. Lucca, V. Poulin, G. F. Abellán, L. Balkenhol, K. Benabed, S. Galli, and R. Murgia, *Phys. Rev. D* **106**, 043526 (2022), arXiv:2202.09379 [astro-ph.CO].
- [207] J. S. Cruz, S. Hannestad, E. B. Holm, F. Niedermann, M. S. Sloth, and T. Tram, *Phys. Rev. D* **108**, 023518 (2023), arXiv:2302.07934 [astro-ph.CO].
- [208] J. S. Cruz, F. Niedermann, and M. S. Sloth, *JCAP* **11**, 033 (2023), arXiv:2305.08895 [astro-ph.CO].
- [209] J. R. Eskilt, L. Herold, E. Komatsu, K. Murai, T. Namikawa, and F. Naokawa, *Phys. Rev. Lett.* **131**, 121001 (2023), arXiv:2303.15369 [astro-ph.CO].
- [210] T. L. Smith and V. Poulin, *Phys. Rev. D* **109**, 103506 (2024), arXiv:2309.03265 [astro-ph.CO].
- [211] R. K. Sharma, S. Das, and V. Poulin, *Phys. Rev. D* **109**, 043530 (2024), arXiv:2309.00401 [astro-ph.CO].

- [212] G. Efstathiou, E. Rosenberg, and V. Poulin, *Phys. Rev. Lett.* **132**, 221002 (2024), arXiv:2311.00524 [astro-ph.CO].
- [213] R. Gsponer, R. Zhao, J. Donald-McCann, D. Bacon, K. Koyama, R. Crittenden, T. Simon, and E.-M. Mueller, *Mon. Not. Roy. Astron. Soc.* **530**, 3075 (2024), arXiv:2312.01977 [astro-ph.CO].
- [214] S. Goldstein, J. C. Hill, V. Iršič, and B. D. Sherwin, *Phys. Rev. Lett.* **131**, 201001 (2023), arXiv:2303.00746 [astro-ph.CO].
- [215] M. Forconi, W. Giarè, O. Mena, Ruchika, E. Di Valentino, A. Melchiorri, and R. C. Nunes, *JCAP* **05**, 097 (2024), arXiv:2312.11074 [astro-ph.CO].
- [216] E. McDonough, J. C. Hill, M. M. Ivanov, A. La Posta, and M. W. Toomey, “Observational constraints on early dark energy,” (2023), arXiv:2310.19899 [astro-ph.CO].
- [217] A. Moss, E. Copeland, S. Bamford, and T. Clarke, “A model-independent reconstruction of dark energy to very high redshift,” (2021), arXiv:2109.14848 [astro-ph.CO].
- [218] G. D’Agostini, *Reports on Progress in Physics* **66**, 1383–1419 (2003).
- [219] R. Trotta (2017) arXiv:1701.01467 [astro-ph.CO].
- [220] R. Trotta, *Contemp. Phys.* **49**, 71 (2008), arXiv:0803.4089 [astro-ph].
- [221] M. Maltoni and T. Schwetz, *Phys. Rev. D* **68**, 033020 (2003), arXiv:hep-ph/0304176.
- [222] S. Gariazzo, O. Mena, and T. Schwetz, *Phys. Dark Univ.* **40**, 101226 (2023), arXiv:2302.14159 [hep-ph].
- [223] L. Amendola and S. Tsujikawa, *Dark Energy: Theory and Observations* (Cambridge University Press, 2015).
- [224] R. E. Kass and A. E. Raftery, *J. Am. Statist. Assoc.* **90**, 773 (1995).
- [225] P. Marshall, N. Rajguru, and A. Slosar, *Phys. Rev. D* **73**, 067302 (2006), arXiv:astro-ph/0412535.
- [226] H. Jeffreys, “The Theory of Probability,” (1939).
- [227] L. Amendola, V. Marra, and M. Quartin, *Mon. Not. Roy. Astron. Soc.* **430**, 1867 (2013), arXiv:1209.1897 [astro-ph.CO].
- [228] M. Raveri and W. Hu, *Phys. Rev. D* **99**, 043506 (2019), arXiv:1806.04649 [astro-ph.CO].
- [229] P. Lemos, F. Köhlinger, W. Handley, B. Joachimi, L. Whiteway, and O. Lahav, *Mon. Not. Roy. Astron. Soc.* **496**, 4647 (2020), arXiv:1910.07820 [astro-ph.CO].
- [230] S. Kullback and R. A. Leibler, *The Annals of Mathematical Statistics* **22**, 79 (1951).
- [231] S. Seehars, A. Amara, A. Refregier, A. Paranjape, and J. Akeret, *Phys. Rev. D* **90**, 023533 (2014), arXiv:1402.3593 [astro-ph.CO].
- [232] A. Nicola, A. Amara, and A. Refregier, *JCAP* **01**, 011 (2019), arXiv:1809.07333 [astro-ph.CO].
- [233] M. Raveri, M. Martinelli, G. Zhao, and Y. Wang, “Information Gain in Cosmology: From the Discovery of Expansion to Future Surveys,” (2016), arXiv:1606.06273 [astro-ph.CO].
- [234] L. Verde, P. Protopapas, and R. Jimenez, *Phys. Dark Univ.* **2**, 166 (2013), arXiv:1306.6766 [astro-ph.CO].
- [235] P. Lemos *et al.* (DES), *Mon. Not. Roy. Astron. Soc.* **505**, 6179 (2021), arXiv:2012.09554 [astro-ph.CO].
- [236] H. Akaike, *IEEE Trans. Autom. Control* **19**, 716 (1974).
- [237] J. Solà Peracaula, J. de Cruz Pérez, and A. Gómez-Valent, *Mon. Not. Roy. Astron. Soc.* **478**, 4357 (2018), arXiv:1703.08218 [astro-ph.CO].
- [238] S. Vagnozzi, S. Dhawan, M. Gerbino, K. Freese, A. Goobar, and O. Mena, *Phys. Rev. D* **98**, 083501 (2018), arXiv:1801.08553 [astro-ph.CO].
- [239] A. Gómez-Valent and L. Amendola, *JCAP* **04**, 051 (2018), arXiv:1802.01505 [astro-ph.CO].
- [240] C. D. Kreisch, F.-Y. Cyr-Racine, and O. Doré, *Phys. Rev. D* **101**, 123505 (2020), arXiv:1902.00534 [astro-ph.CO].
- [241] P. Agrawal, F.-Y. Cyr-Racine, D. Pinner, and L. Randall, *Phys. Dark Univ.* **42**, 101347 (2023), arXiv:1904.01016 [astro-ph.CO].
- [242] L. Visinelli, S. Vagnozzi, and U. Danielsson, *Symmetry* **11**, 1035 (2019), arXiv:1907.07953 [astro-ph.CO].
- [243] S. Roy Choudhury and S. Hannestad, *JCAP* **07**, 037 (2020), arXiv:1907.12598 [astro-ph.CO].
- [244] N. Aghanim *et al.* (Planck), *Astron. Astrophys.* **641**, A5 (2020), arXiv:1907.12875 [astro-ph.CO].
- [245] A. G. Riess *et al.*, *Astrophys. J. Lett.* **934**, L7 (2022), arXiv:2112.04510 [astro-ph.CO].
- [246] J. Torrado and A. Lewis, *JCAP* **05**, 057 (2021), arXiv:2005.05290 [astro-ph.IM].
- [247] A. Lewis and A. Challinor, *Phys. Rev. D* **76**, 083005 (2007), arXiv:astro-ph/0702600 [ASTRO-PH].
- [248] A. Challinor and A. Lewis, *Phys. Rev. D* **84**, 043516 (2011), arXiv:1105.5292 [astro-ph.CO].
- [249] C. Howlett, A. Lewis, A. Hall, and A. Challinor, *JCAP* **1204**, 027 (2012), arXiv:1201.3654 [astro-ph.CO].
- [250] A. Lewis, A. Challinor, and A. Lasenby, *Astrophys. J.* **538**, 473 (2000), arXiv:astro-ph/9911177.
- [251] J. Lesgourgues, arXiv e-prints , arXiv:1104.2932 (2011), arXiv:1104.2932 [astro-ph.IM].
- [252] D. Blas, J. Lesgourgues, and T. Tram, *JCAP* **2011**, 034 (2011), arXiv:1104.2933 [astro-ph.CO].
- [253] A. Lewis and S. Bridle, *Phys. Rev. D* **66**, 103511 (2002), arXiv:astro-ph/0205436.
- [254] R. M. Neal, “Taking bigger metropolis steps by dragging fast variables,” (2005), arXiv:math/0502099 [math.ST].
- [255] A. Gelman and D. B. Rubin, *Statist. Sci.* **7**, 457 (1992).
- [256] C. Cartis, J. Fiala, B. Marteau, and L. Roberts, arXiv e-prints , arXiv:1804.00154 (2018), arXiv:1804.00154 [math.OC].
- [257] C. Cartis, L. Roberts, and O. Sheridan-Methven, arXiv e-prints , arXiv:1812.11343 (2018), arXiv:1812.11343 [math.OC].
- [258] M. Powell, Technical Report, Department of Applied Mathematics and Theoretical Physics (2009).
- [259] A. Heavens, Y. Fantaye, A. Mootoovaloo, H. Eggers, Z. Hosenie, S. Kroon, and E. Sellentin, “Marginal Likelihoods from Monte Carlo Markov Chains,” (2017), arXiv:1704.03472 [stat.CO].